Supplementary Information (SI) for Journal of Materials Chemistry A.

SUPPORTING INFORMATION

Poly(styrene-co-maleamic acid)-based Monoamide Covalent Adaptable Networks

*Aitor Hernández, Susanne M. Fischer, Johan M. Winne and Filip E. Du Prez**

Polymer Chemistry Research Group, Centre of Macromolecular Chemistry, and Laboratory for Organic Synthesis, Department of Organic and Macromolecular Chemistry, Faculty of Sciences, Ghent University, Krijgslaan 281 S4, Ghent B-9000, Belgium.

* E-mail: Filip.DuPrez@UGent.be

Table of Contents

1. *Reagents and Chemicals*

Acetic acid (glacial) ≥ 99 % (Chemlab, CAS: 64-19-7), acetic anhydride ≥ 98.0 % (Sigma-Aldrich, CAS: 108-24-7), benzoic acid ≥ 99.5 % (Sigma-Aldrich, CAS: 65-85-0), n-butyl acetate (puriss. p.a.) ≥ 99.5 % (Sigma-Aldrich, CAS: 123-86-4), chloroform-d 99.80 % D (Eurisotop, CAS:865-49-6), dichloromethane ≥ 99.8 % (Sigma-Aldrich, CAS: 75-09-2), diethyl ether ≥ 99.5 % (Fischer Scientific, CAS: 60-29-7), N,N-dimethyl-1,6-hexanediamine > 97.0 % (TCI Chemicals, CAS: 13093-04-4), methanol ≥ 99.8 % (Fischer Scientific, CAS: 67-56-1), 7-Methyl-1,5,7-triazabicyclo(4.4.0)dec-5-ene > 95.0 % (TCI Chemicals, CAS: 84030-20-6), piperidine ≥ 99 % (Sigma-Aldrich, CAS: 110-89-4), succinic anhydride ≥ 99 % (Sigma-Aldrich, CAS: 108-30-5), tetrahydrofuran ≥99.8 % (Fischer Scientific, CAS: 109-99-9), p-toluenesulfonic acid (monohydrate) ≥ 98.5 % (Sigma-Aldrich, CAS: 6192-52-5), 4,4'-trimethylenedipiperidine 97 % (Sigma-Aldrich, CAS: 16898-52-5), Xibond® 120 (kindly provided by Polyscope), Xibond® 220 (kindly provided by Polyscope) and zinc acetate (anhydrous) > 99.8 % (Alfa Aesar, CAS: 557-34-6).

All reagents and solvents were used as received from their supplier with the exception of succinic anhydride and maleic anhydride containing copolymers, which were dried for at least 2 h under vacuum at 60°C and 120°C respectively, prior to their use.

2. *Characterization Methods and Instrumentation*

Gel Permeation Chromatography (GPC) analyses were performed on a Varian PLGPC50plus instrument using a Waters 2414 Refractive Index detector, equipped with a GPC precolumn PSS SDV analytical 5 µ 8,0 x 50 mm, three PSS SDV analytical 5 µm columns comprising a 1000 - 1000000 Å range and a Waters 1500 Column Oven stabilized at 35°C. Narrow polystyrene standards of 1.930.000, 758.500, 370.000, 130.000, 72.900, 28.770, 21.720, 9.920, 4.910, 2.450, 1.280 and 580 g/mol were used for calibration and the samples from solutions of 5 mg/mol in chloroform were injected using a Waters 717plus autosampler at solvent flow rate of 1 mL min^{-1}. The obtained molar mass distributions were then processed using the Waters Breeze software to calculate number average molar masses (M_n), weight average molar masses (M_n) and dispersities (Đ).

^{1}H and ^{13}C nuclear magnetic resonance (NMR) spectra were recorded using a Bruker Avance 300 (300 MHz) or Bruker Ascend 400 (400 MHz). The NMR chemical shifts were reported as δ in parts per million (ppm) relative to the traces of non-deuterated solvent (δ = 7.26 for $CDCl_3$). Standard applied parameters (number of scans, pulse delay, acquisition time, tilt angle, pulse time): ^{1}H spectra (300 MHz: ns = 16, D1 = 1.0 s, AQ = 2.65 s, 30°, P1 = 7.25 µs. The NMR chemical shifts were reported as δ in parts per million (ppm) relative to the traces of non-deuterated solvent (δ = 7.26 for $CDCl_3$ and δ = 2.50 for DMSO). Data were reported as follows: chemical shift, multiplicity (s = singlet, d = doublet, t = triplet, q = quadruplet, p = quintuplet, h = hextuplet, hept = heptuplet, m = multiplet, br = broad), coupling constants (J) given in Hertz (Hz), and integration values. Applied parameters (number of scans, pulse delay, acquisition time, tilt angle, pulse time): ^{1}H spectra (300

MHz: ns = 16, D1 = 1.0 s, AQ = 2.65 s, 30°, P1 = 7.25 µs; 400 MHz: ns = 16, D1 = 1.0 s, AQ = 4.10 s, 30°, P1 = 7.75 µs); ^{13}C spectra (300 MHz: ns = 3072, D1 = 2.0 s, AQ = 1.82 s, 30°, P1 = 7.50 µs; 400 MHz: ns = 3072, D1 = 2.0 s, AQ = 1.36 s, 30°, P1 = 7.50 µs).

Attenuated total reflectance - Fourier transform infrared (ATR-FTIR) spectra were collected on a PerkinElmer Spectrum 1000 FTIR spectrometer equipped with Pike ATR module on a room kept at 21°C and 1 atm. Spectra were recorded between 4000-600 cm^{-1} with a spectrum resolution of 4 cm^{-1}. All spectra were averaged over 16 scans.

High temperature (attenuated total reflectance) - FTIR (HT-FTIR) spectra were collected in attenuated total reflectance mode on a PerkinElmer Spectrum 1000 FTIR spectrometer equipped with Pike ATR module. The measured sample (code **LMe$_{50}$**, see **Table S1** for formulation) consisted of 2 mm thickness 8 mm diameter discs cut from plates hot-pressed at 190°C. The temperatures starting at 100°C and up to 200°C were equilibrated for 10 min before the acquisition of the spectra (32 scans).

Differential scanning calorimetry (DSC) measurements were performed on a Mettler Toledo 1/700 calorimeter equipped with a full range sensor (FRS5) sensor containing 56 thermocouples, liquid nitrogen cooling system enabling a temperature range of -150°C to 700°C and automatic sample robot. All measurements were conducted under a nitrogen atmosphere in perforated standard 40 µL aluminum crucibles containing 5 – 15 mg of polymeric material. A consecutive heating-cooling-heating run was performed in a temperature range of -25°C to 200°C at a heating rate of 10°C min^{-1} followed by a cooling rate of 1°C min^{-1} to ensure a progressive and slow shift in the dissociative equilibrium that would allow a reproducible result. Then the analyzed heating run from 25°C to 225°C was recorded at 10°C min^{-1}. The obtained thermograms were analyzed with the STARe Excellence Software and the reported glass transition temperature (T_g) was determined as the midpoint from the second heating run at 10°C min^{-1}, which is defined as the intercept of the DSC curves and the bisector of the angle formed by the extrapolation of the baselines before and after the transition.

Thermogravimetric analyses (TGA) were performed on a Mettler Toledo TGA/SDTA851e equipped with a Julabo FP50 circulator with HP control unit which is calibrated using three indium pills and ≈6 mg aluminum. Samples were placed in ceramic pans and heated from 25°C up to 800°C at 10°C min^{-1} under nitrogen atmosphere or air. The obtained thermograms were analyzed with the STARe Excellence Software and the onset temperature of degradation was defined at 2 % weight loss.

Rheology measurements were conducted with a modular compact rheometer (MCR) 302 from Anton Paar containing an air-bearing-supported synchronous electrically commutated (EC) motor, integrated normal force sensor, TruRate^{TM} sample adaptive controller, TruStrain^{TM} real-time position control and a Convection

Temperature Device 180 (CTD 180) heating unit. Measurements were designed and analyzed by making use of the RheoCompass$^{\mathrm{TM}}$ software. All experiments were performed in rough parallel plate geometry using 8 mm sample disks, using a normal force of 1 N while monitoring the gap between each plate and the applied stress was always comprised in the linear viscoelastic region at the measured temperatures. For Small Amplitude Oscillatory Shear (SAOS) frequency sweep experiments, the shear storage ($G'(\omega, T)$) and loss ($G'(\omega, T)$) moduli were followed over time at constant temperatures at a set strain of 2.0%. On *Stress Relaxation* measurements the relaxation modulus ($G(t, T)$) was followed over time at constant temperature using a constant shear strain of 1%, within the linear viscoelastic region of the samples. Unless specified, all series of stress relaxation experiments at different temperatures were performed successively on the same sample always starting the set at the highest indicated temperature. Prior to *Creep* experiments, the samples were annealed at 180°C for 5 min and then cooled down from 180°C to 100°C to remove their thermal history. For each single creep measurement, the shear strain ($\gamma(t)$) and creep compliance ($J(t, T) = \gamma(t, T)/\sigma$) were followed. After each consecutive temperature was reached, the sample was kept with no applied stress (σ) for 300 s to be then subjected to a constant shear stress (of 1000 Pa for MeHDA- based networks and 2000 Pa for DPP-based networks respectively). All creep measurements were conducted successively on the same sample starting at the lowest temperatures (ranging from 120°C to 215°C).

Network (re)processing by compression molding *was performed with s*amples consisting of shredded network plates obtained *via* compression molding, which were processed by compression molding at 190°C for 10 min applying 7 MPa over the used rectangular mold (A: 70 mm x 40 mm x 2 mm; B: 30 mm x 15 mm x 2 mm) to yield colorless transparent plates (**Scheme 1.C)**.

Injection molding experiments were performed using a DSM Mini Injection Molding machine following these injection parameters: sample heating time 2 min at 280°C, mold temperature set to 80, 140 or 180°C, injection die diameter of 5mm, and 8 bar injection pressure held for 10 s after mold filling . Then the injected rectangular specimen was immediately extracted from the mold (**Figure 8**) without further treatment. The dimensions of the mold were 63.5 mm x 12.5 mm x 3.15 mm connected through a semicircular filling conduct of 1.1 mm radius.

Dynamic mechanical thermal analysis (DMTA). Experiments on a dual cantilever setup mode were conducted using a DMA/SDTA861 from Mettler-Toledo equipped with a shear clamp setup holding two 8 mm diameter and 0.97 mm thickness sample discs. To determine the storage *(*$G'(f, T)$*)* and loss *(*$G''\ (\omega, T)$*)* moduli values the experiments were conducted with a temperature ramp from 25°C up to 275°C, heating rate of 3°C/min, , frequency of 1 Hz, a displacement amplitude set to 0.54% and a geometry factor of 9.6488 1/m. During each experiment, 20 datapoints per decade were collected on a logarithmic scale.

GPC analysis

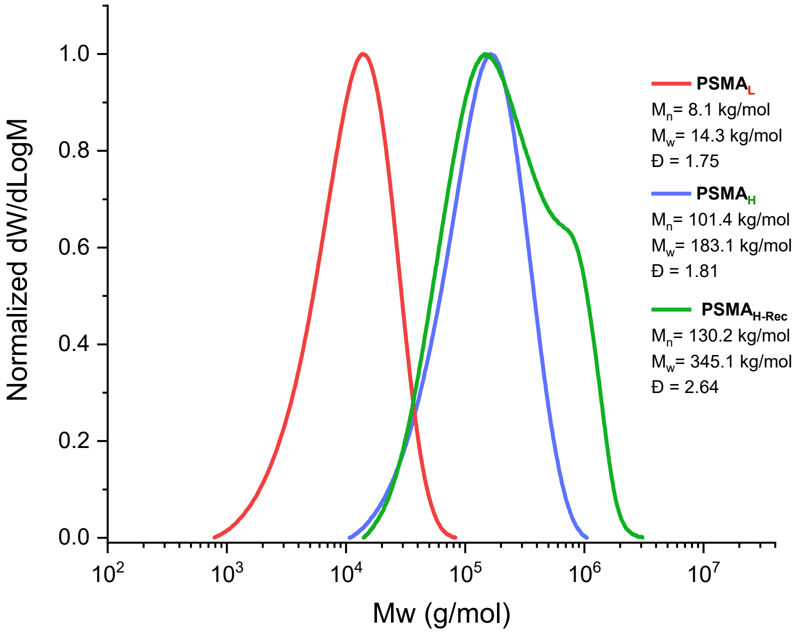

Figure S1. GPC chromatograms and results of virgin **PSMA$_L$** (red), **PSMA$_H$** (cyan) and a sample of **PSMA$_{H\text{-}Rec}$** (green) recuperated via chemical recycling procedures measured in $CHCl_3$.

3. Synthetic procedures

Table S1. Formulations used in the syntheses of **PSMA$_L$** derived PS-MMAs.

Network	[NH]/[MA] eq/eq	PSMA$_L$ (g)	MA (mmol)	MA (g)	Crosslinker	Crosslinker (mmol)	Crosslinker (g)
LMe$_{50}$	0.50	10.0	10.71	1.05	MeHDA	2.68	0.39
LMe$_{100}$	1.00	10.0	10.71	1.05	MeHDA	5.35	0.77
LDP$_{50}$	0.50	10.0	10.71	1.05	DPP	2.68	0.56

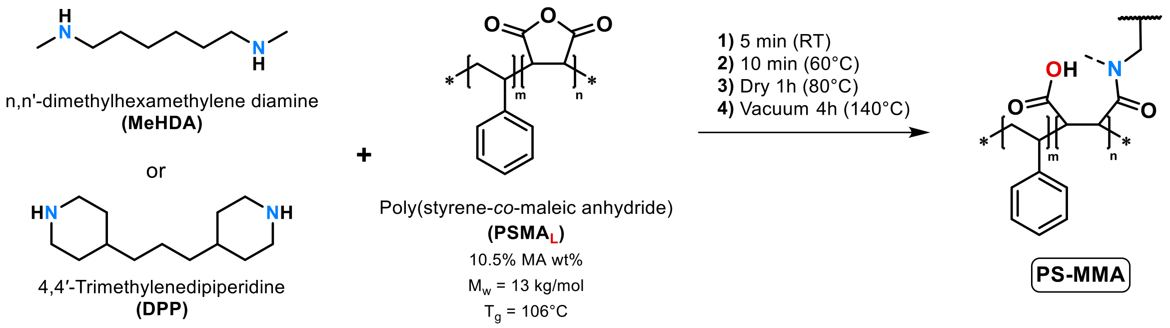

Scheme S1. Schematic representation of the synthesis of **PSMA$_L$** derived PS-MMAs.

Table S2. Formulations used in the syntheses of **$PSMA_H$**-derived PS-MMAs

Network	**[NH]/[MA]** eq/eq	**$PSMA_{H13}$** (g)	**MA** (mmol)	**MA** (g)	**Crosslinker**	**Crosslinker** (mmol)	**Crosslinker** (g)
HMe_{10}	0.10	20.00	17.74	1.74	MeHDA	1.77	0.26
HMe_{50}	0.50	10.00	8.87	0.87	MeHDA	4.44	0.64
HDP_{10}	0.10	200.00	177.45	17.40	DPP	8.87	1.87
HDP_{50}	0.50	20.00	17.74	1.74	DPP	4.44	0.93

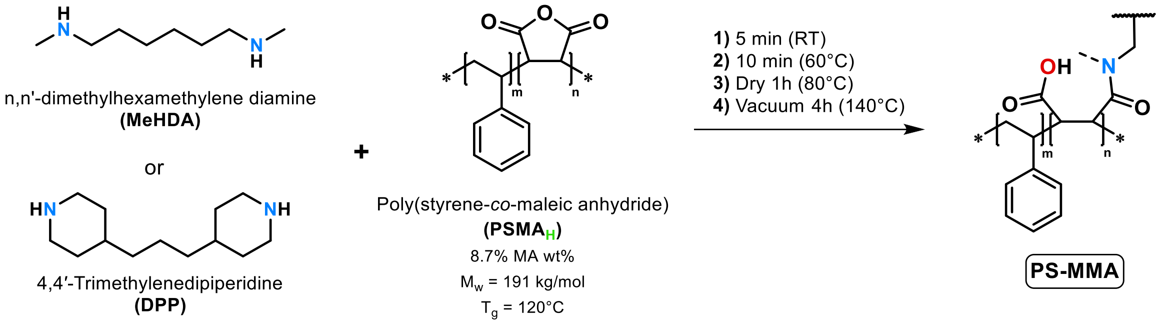

Scheme S2. Schematic representation of the synthesis of **$PSMA_H$** derived PS-MMAs.

Table S3. Formulations used in the synthesis of **HMe_{50}** PS-MMA networks doped with external reptation stickers.

Sticker	**$PSMA_L$** **(g)**	**MA** **(mmol)**	**MA** **(g)**	**Crosslinker**	**Crosslinker** **(mmol)**	**Crosslinker** **(g)**	**Sticker** **(mmol)**	**Sticker** **(g)**
BzOH	10.00	8.87	0.87	MeHDA	2.22	0.32	1.11	0.14
pTSOH	10.00	8.87	0.87	MeHDA	2.22	0.32	1.11	0.19
$ZnAc_2$	10.00	8.87	0.87	MeHDA	2.22	0.32	1.11	0.20
MeTBD	10.00	8.87	0.87	MeHDA	2.22	0.32	1.11	0.17

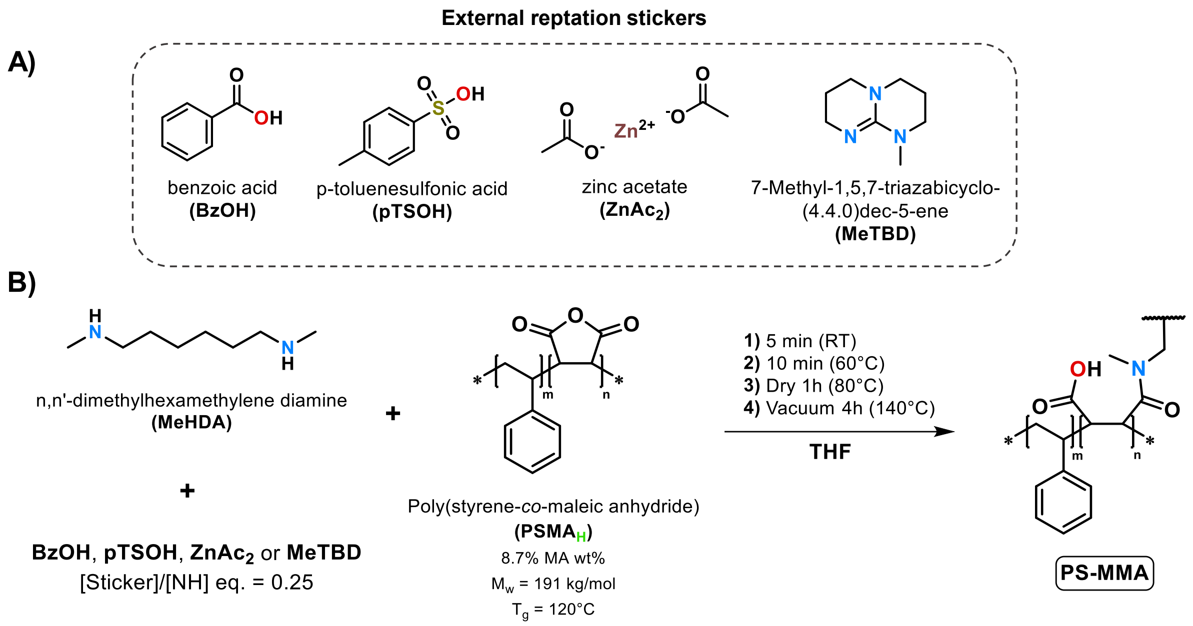

Scheme S3. A) External reptation stickers used to dope **HMe₅₀** samples. **B)** Schematic representation of the synthesis of **HMe₅₀** PS-MMA networks doped with external reptation stickers.

Table S4. Formulations used in the synthesis of **HMe₅₀** PS-MMA networks doped with external reptation stickers.

Sticker[a]	PSMA	Crosslinker	[NH]/[MA] (eq/eq)	[Sticker]/[MA] (eq/eq)	T_g[b] (°C)	$T_{d2\%}$[c] (°C)	Swelling ratio (wt%)	Soluble fraction (wt%)
None	$PSMA_H$	MeHDA	0.50	-	132	342	90 ± 8	4.8 ± 0.7
BzOH	$PSMA_H$	MeHDA	0.50	0.25	130	294	68 ± 3	5.0 ± 0.9
pTSOH	$PSMA_H$	MeHDA	0.50	0.25	124	340	88 ± 5	8.7 ± 3.0
$ZnAc_2$	$PSMA_H$	MeHDA	0.50	0.25	127	321	166 ± 8	6.8 ± 1.5
MeTBD	$PSMA_H$	MeHDA	0.50	0.25	132	288	90 ± 8	4.8 ± 0.7

[a] External reptation sticker added to the **HMe₅₀** network. [b] Glass transition temperature (T_g) obtained from the second heating run measured by DSC (**Figure S3.C**). [c] Onset temperature after 2% mass loss measured by TGA (**Figures S4.C,S5.B**).

Synthesis of PP-MMA model monoamide

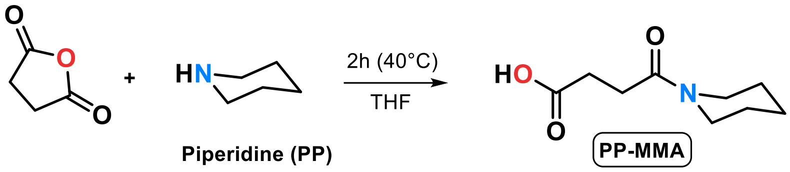

Scheme S4. Schematic representation of the synthetic procedure of **PP-MMA** .

The synthesis of 4-oxo-4-(piperidin-1-yl)butanoic acid (**PP-MMA**) was performed in a single step reaction. In a 50mL single neck round bottom flask kept in an oil bath at room temperature and equipped with a magnetic stirrer, 30 mL of THF was added and kept under continuous stirring until the end of the procedure. Then, succinic anhydride (1.50g , 14.99 mmol, 1.00 eq.) was added to the flask, followed by piperidine (PP) added dropwise (1.34 g, 15.74 mmol, 1.05 eq.). Once the amine was added a waterless condenser was equipped to the setup and the temperature of the bath was raised and kept at 40°C for 2 h. The colorless reaction mixture was concentrated under reduced pressure and then 100 mL of EtOAc was added to it. Then the solution was extracted two times with 30mL of NaOH (1M) solution and one last time with 10 mL of distilled water. Lastly the organic phase was dried over $NaSO_4$ and dried under vacuum yielding a colorless and crystalline solid.

PP-MMA: Light yellow oil (2.41 g, 87 % yield). ^{1}H-NMR (400 MHz, chloroform-d): δ = 1.40 – 1.65 (m, 6H), 2.60 – 2.70 (s, 4H, NH), 3.30–3.50 (t, 2H), 3.55–3.65 (t, 2H), 9.00 – 9.50 (br, 1H) . ^{13}C-NMR (400 MHz, chloroform-d) δ 24.48, 25.58, 26.39, 28.18, 29.96, 43.30, 46.73, 170.34, 176.53. The structure matches data reported in the literature.[1]

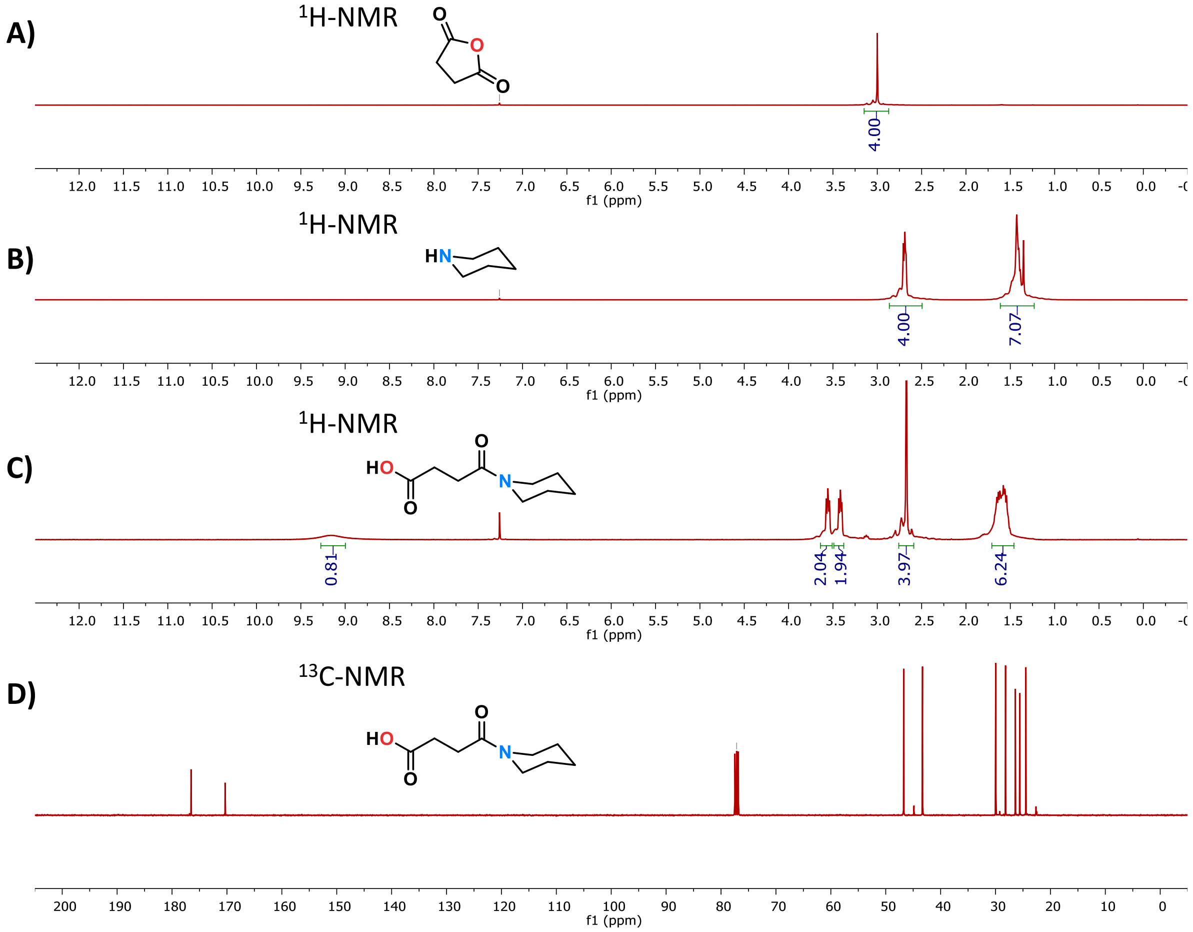

Figure S2 ^{1}H-NMR spectra of **A)** Succinic anhydride, **B)** Piperidine and **C)** PP-MMA and ^{13}C-NMR spectrum of **D) PP-MMA**.

4. Thermal analyses

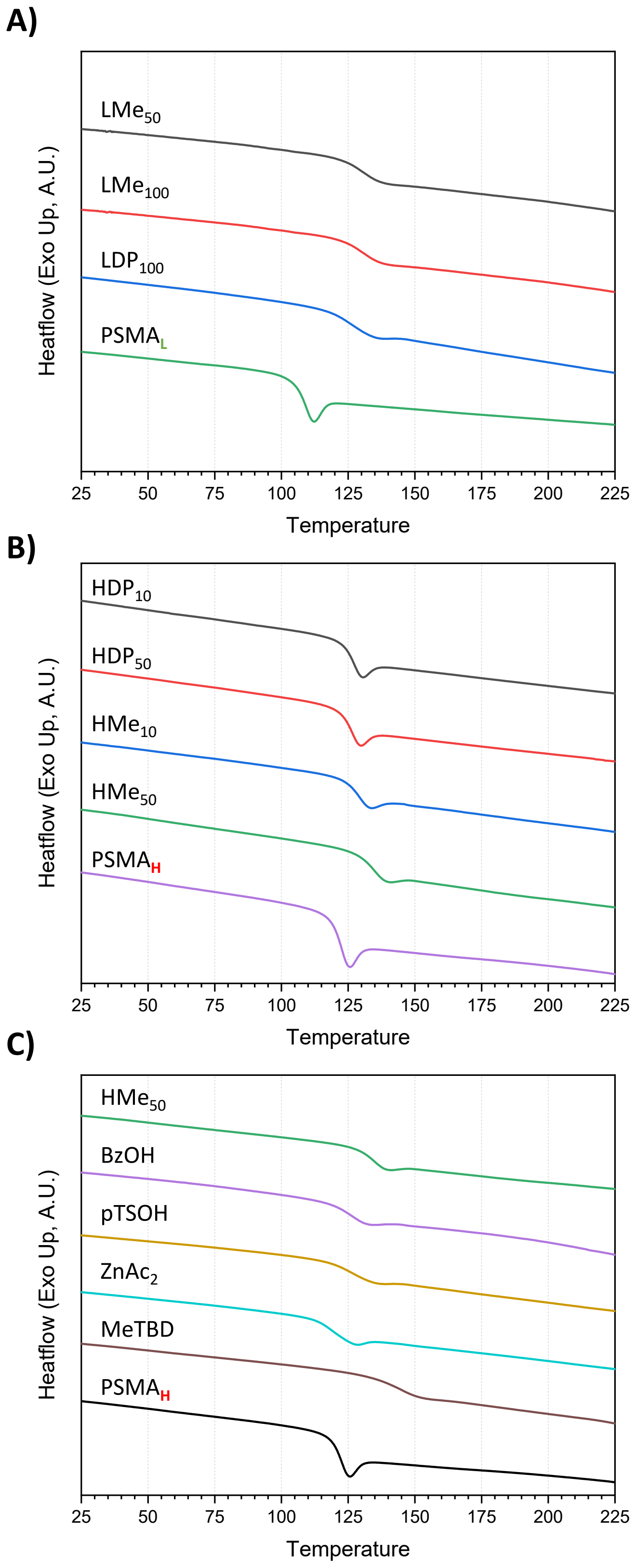

Figure S3. DSC thermograms of: **A)** PS-MMA networks derived from $\mathbf{PSMA_L}$. **B)** PS-MMA networks derived from $PSMA_H$. **C)** Network $\mathbf{HMe_{50}}$ and $\mathbf{HMe_{50}}$ samples doped with different external reptation stickers.

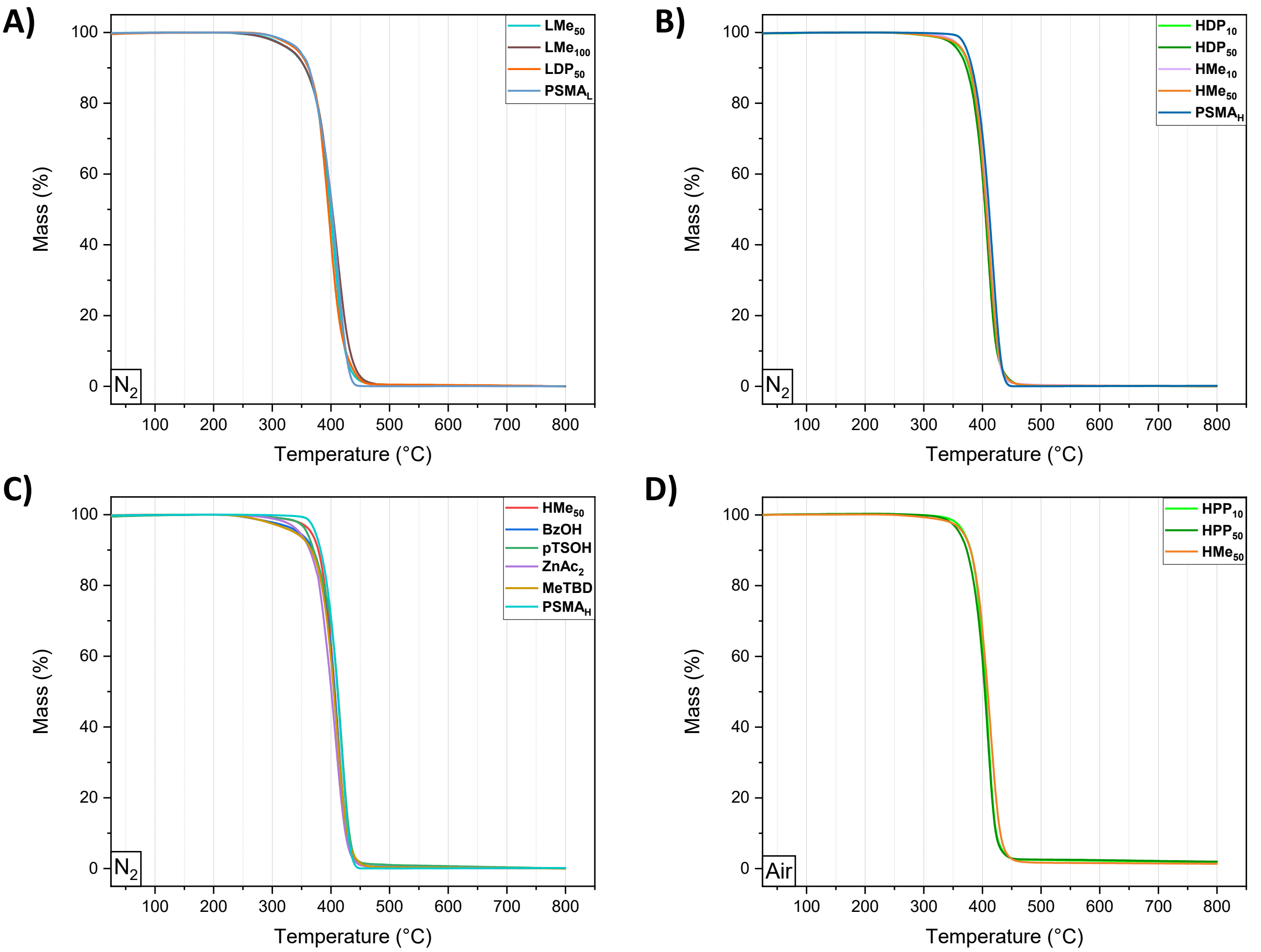

Figure S4. Dynamic TGA thermograms performed from 25°C to 800°C under nitrogen atmosphere of reference of: **A)** PS-MMA networks derived from **PSMA$_L$**. **B)** PS-MMA networks derived from **PSMA$_H$**. **C)** Network **HMe$_{50}$** and **HMe$_{50}$** samples doped with different external reptation stickers. **D)** Dynamic TGA thermograms performed from 25°C to 800°C under standard air atmosphere of networks **HDP$_{10}$**, **HDP$_{50}$** and **HMe$_{50}$**.

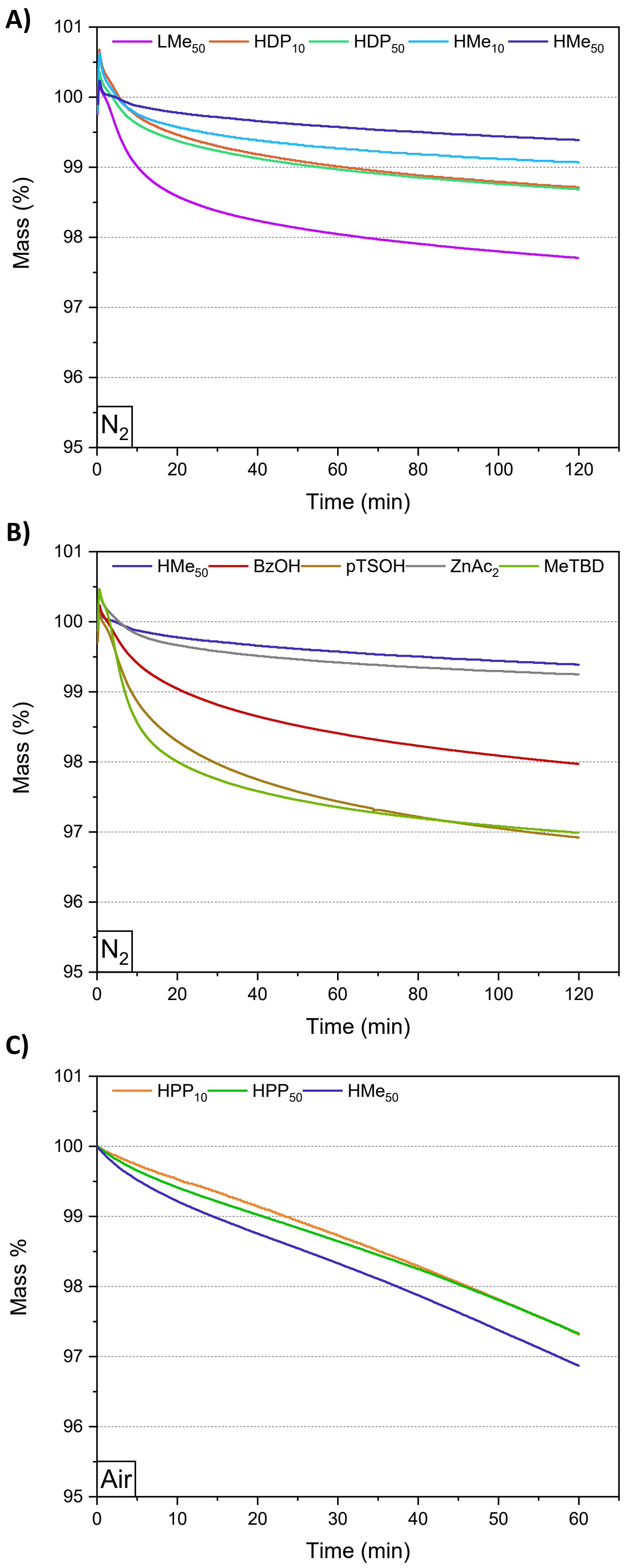

Figure S5. Isothermal TGA of thermograms performed at 250°C under nitrogen atmosphere of: **A)** PS-MMA networks derived from PSMA$_H$ and **LMe$_{50}$** network as reference of the PSMAL-derived materials. **B)** Network **HMe$_{50}$** and **HMe$_{50}$** samples doped with different external reptation stickers. **C)** Isothermal TGA of thermograms performed at 280°C under standard air atmosphere of networks **HDP$_{10}$**, **HDP$_{50}$** and **HMe$_{50}$**.

5. Rheological measurements

5.1. Oscillatory measurements - SAOS

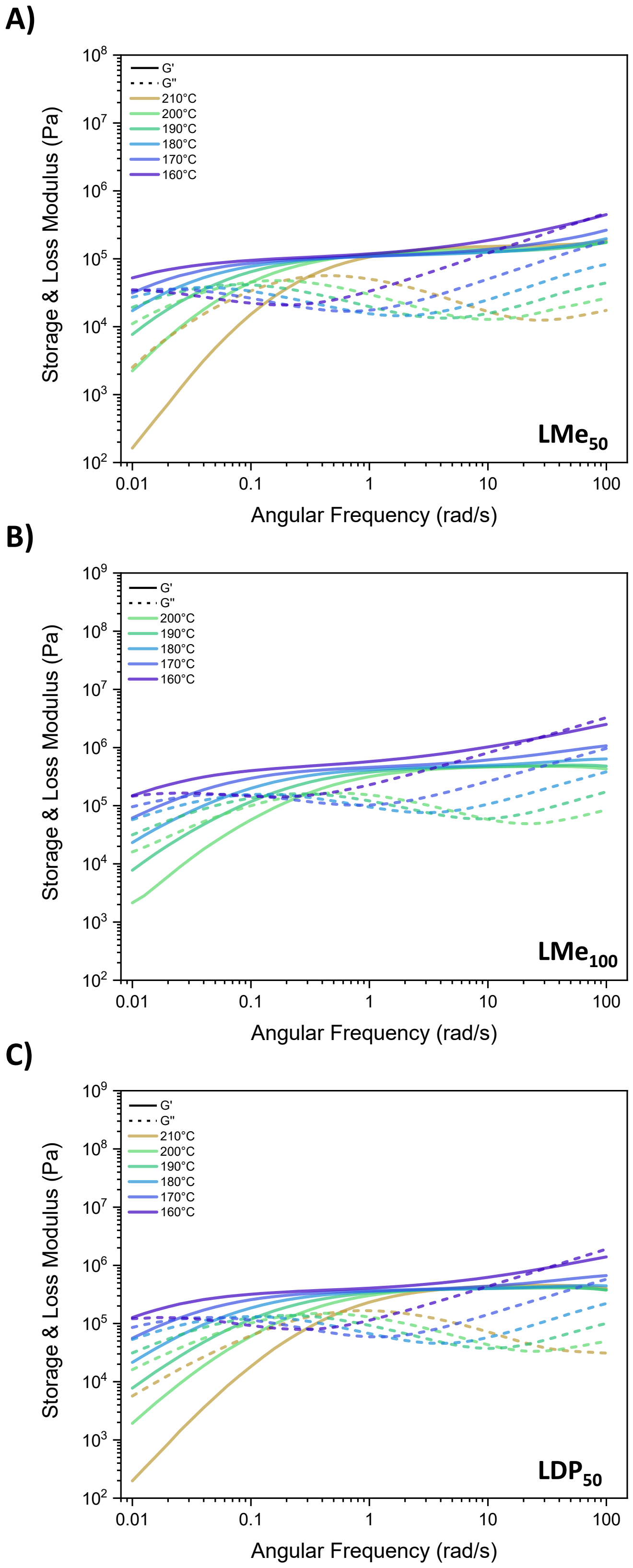

Figure S6. SAOS Frequency sweep measurements at temperatures ranging from 210°C or 200°C to 160°C of **PSMA$_L$**-derived PS-MMA networks: **A) LMe$_{50}$, B) LMe$_{100}$** and **C) LDP$_{50}$**.

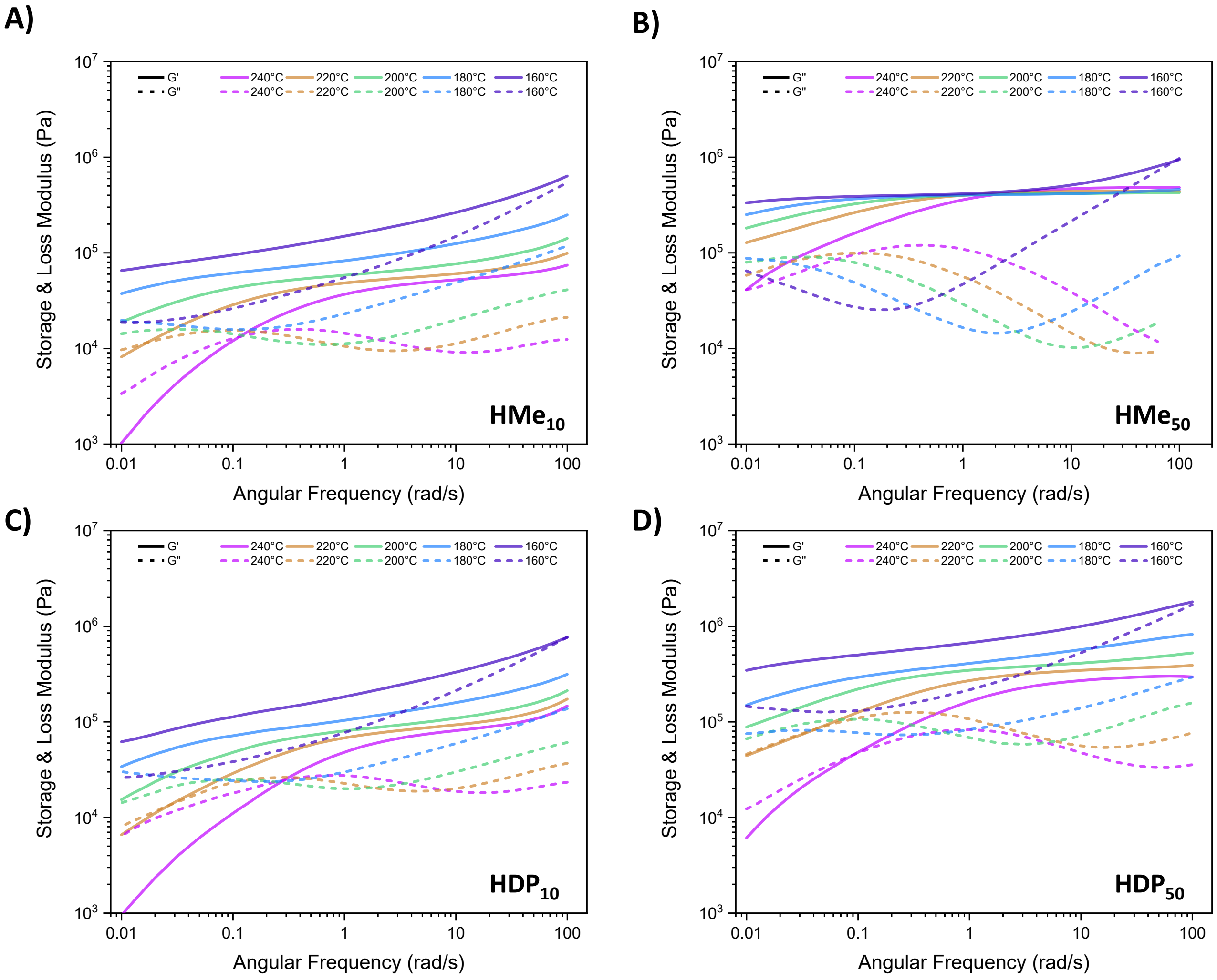

Figure S7. SAOS frequency sweep measurements at temperatures ranging from 240°C to 160°C of **$PSMA_H$**-derived PS-MMA networks: **A) HMe_{10}**, **B) HMe_{10}**, **C) HDP_{10}** and **D) HDP_{50}**.

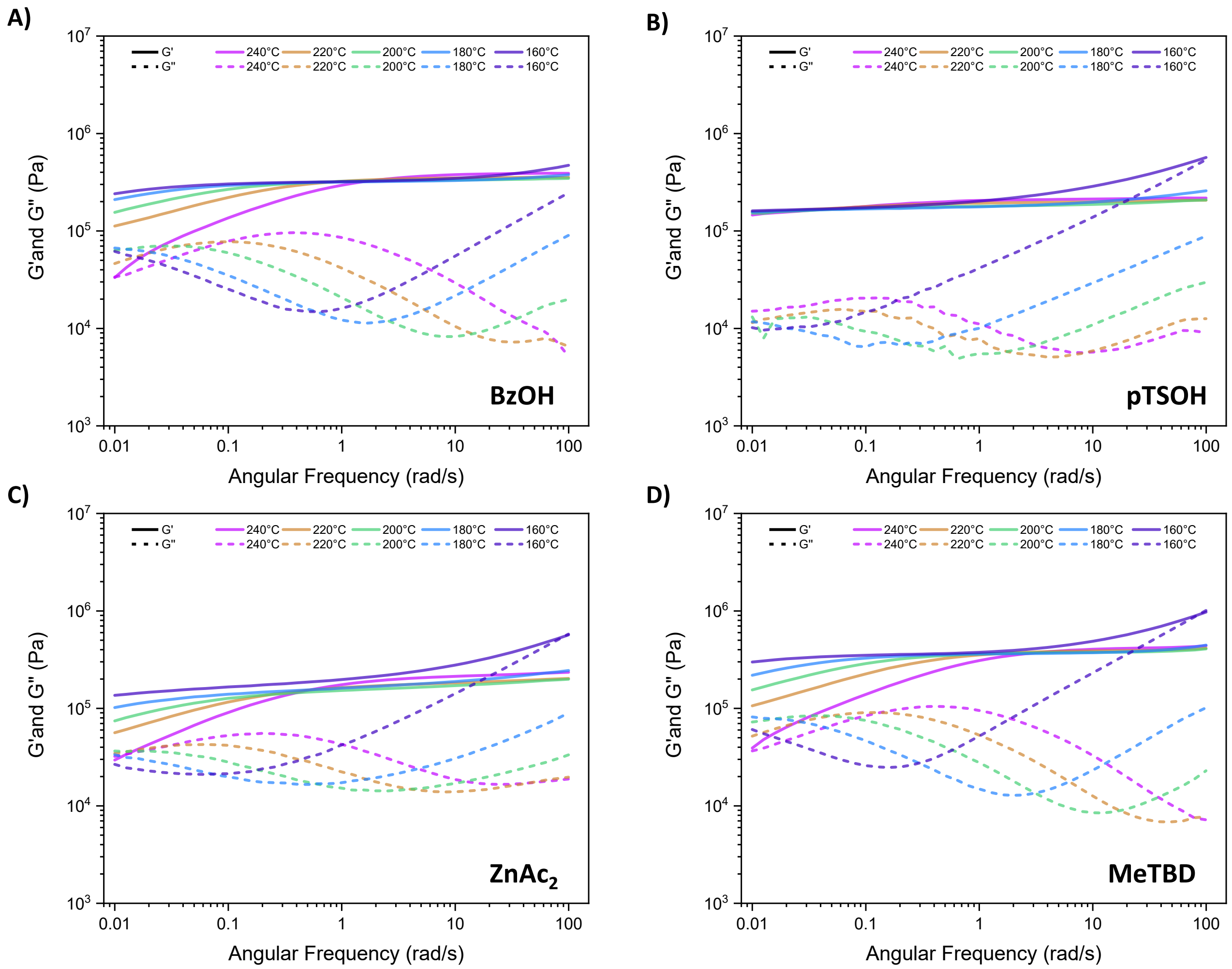

Figure S8. SAOS Frequency sweep measurements at temperatures ranging from 240°C to 160°C of network **HMe$_{50}$** samples doped with different external reptation stickers: **A)** BzOH, **B)** pTSOH, **C)** ZnAc$_2$ and **D)** MeTBD.

5.2. Stress relaxation measurements

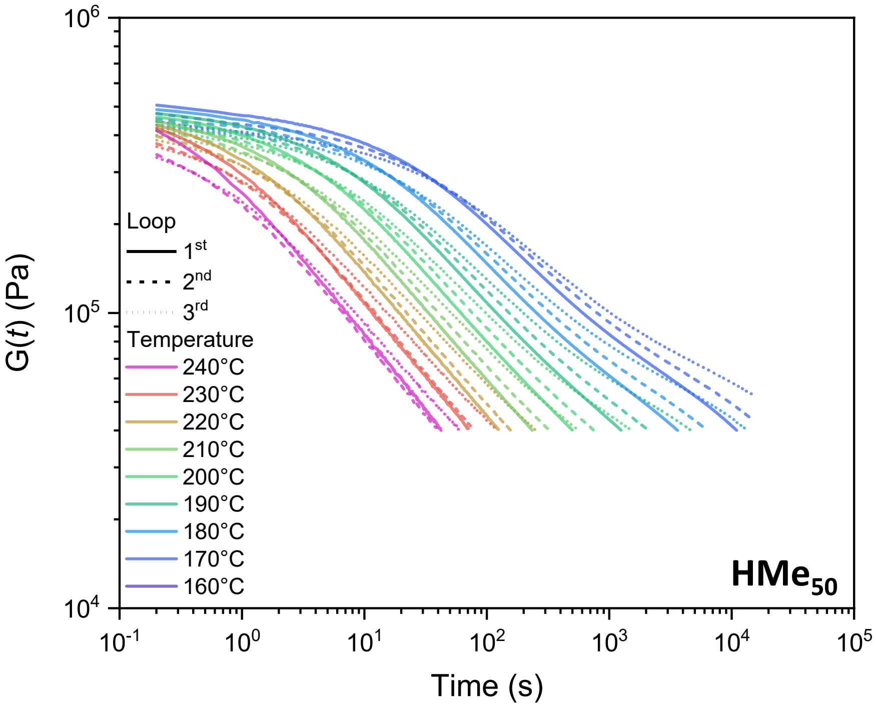

Figure S9. Three consecutive stress relaxation loops performed from 240 to 160°C on a **HMe50** sample, showing no major flow property losses.

The following fittings (**Figures S10**) were made using the Kohlrausch–Williams–Watts (KWW) stretched exponential decay ($Eq. S1$)[2–4] and continuous relaxation spectra (CRS, see $Eq. S2$).

On the one hand the KKW model considers a range of similar relaxation mechanisms of slightly variable speeds using the correction constant β (see **Table S5**), which also contributes to further necessary adjustments associated to viscosity changes resulting from mobility increments experienced by the PSMA chain segments as temperature rises. In the KWW equation, β ranges between 0 and 1, ***(G(t,T))*** represents the relaxation modulus of the system at time t in seconds and temperature T in Kelvin, G_0 is the relaxation modulus at (t = 0) and τ is the relaxation time of the system at a given temperature.

On the other hand, in CRS spectra (obtained using open-source software package 'pyReSpect'),[5] ($G(t, T)$) ($Eq. S2$) represents the relaxation modulus of the system at a constant temperature T in Kelvin. Then, the resulting $H(\lambda)$ distributions (**Figures S11,S**) represent the distribution of relaxation strengths as a function of the relaxation times λ.[6] However, since the continuous analysis on noisy datasets would interfere with the calculation of the relaxation modes of the system, these analyses were performed on denoised stress relaxation curves (unlike on the aforementioned KWW fittings).

$$G(t,T) = G_0 . e^{-\left(\frac{t}{\tau^*}\right)^{\beta}} \qquad (Eq.S1)$$

$$G(t,T) = \int_{-\infty}^{\infty} H(\lambda)\, e^{-\frac{t}{\tau}}\, d\ln\lambda \ = \ \int_{-\infty}^{\infty} \frac{H(\lambda)}{\tau}\, e^{-\frac{t}{\lambda}}\, d\lambda \quad (\mathrm{Eq.S2})$$

$$\tau(T) = A.e^{\left(\frac{E_{a,k}}{RT}\right)} \qquad (Eq.S3)$$

Table S5. Stress relaxation β values calculated by fitting the curves to a Kohlrausch–Williams–Watts (KWW) stretched exponential decay equation ($E_{a,k}$).

Material	**Temperature (°C)**												
	160	**165**	**170**	**175**	**180**	**185**	**190**	**195**	**200**	**205**	**210**	**215**	**220**
LMe$_{50}$	0.52	0.53	0.54	0.54	0.54	0.55	0.55	0.55	0.55	0.55	0.55	0.55	0.56
LMe$_{100}$	0.45	0.46	0.46	0.46	0.47	0.47	0.46	0.46	0.46	0.46	0.46	0.45	0.47
LDP$_{50}$	0.48	0.50	0.51	0.52	0.52	0.52	0.52	0.52	0.52	0.51	0.51	0.51	0.51

Table S6. Rheological properties of **L**-Series PS-MMA networks obtained *via* stress relaxation measurements.

Material	$\tau_{200°C}$[a] (s)		$\tau_{180°C}$[b] (s)		E_{ak}[c] (kJ.mol^{-1})	R^2[d]	E_{ak}[e] (kJ.mol^{-1})	R^2[f]
	KWW	**CRS**	**KWW**	**CRS**	**KWW**		**CRS**	
LMe$_{50}$	0.4	0.9	6	13	120 ± 1.3	0.999	126 ± 1.5	0.999
LMe$_{100}$	0.3	1.3	8	17	120 ± 0.4	1.00	132 ± 0.4	0.999
LDP$_{50}$	0.2	0.5	3	7	123 ± 1.9	0.998	132 ± 0.5	1.00

[a, b] Relaxation times τ at 200°C or 180°C obtained from CRS $H(\lambda)$ maxima and KWW fittings. [c,e] Kinetic activation energy ($E_{a,k}$) of the stress relaxation of the network calculated from the fitting of its KWW or CRS $\tau(T)$ to equation ($Eq.S3$). [d, f] Coefficient of determination (R^2) of the fittings used to calculate the $E_{a,k}$ of the networks.

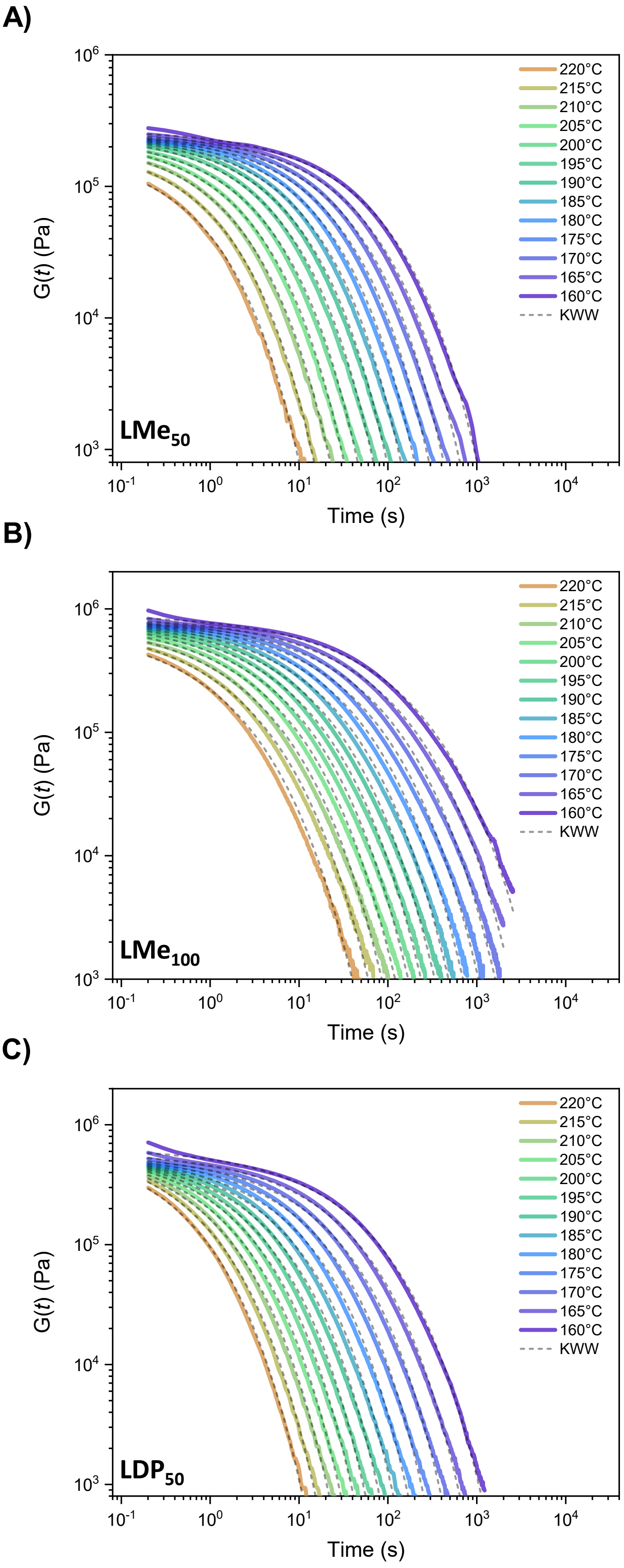

Figure S10. Stress relaxation curves performed at temperatures ranging from 220°C to 160°C of networks: **A) LMe$_{50}$**, **B) LMe$_{100}$**, and **C) LDP$_{50}$** with the corresponding KWW fitted curves (dash lines).

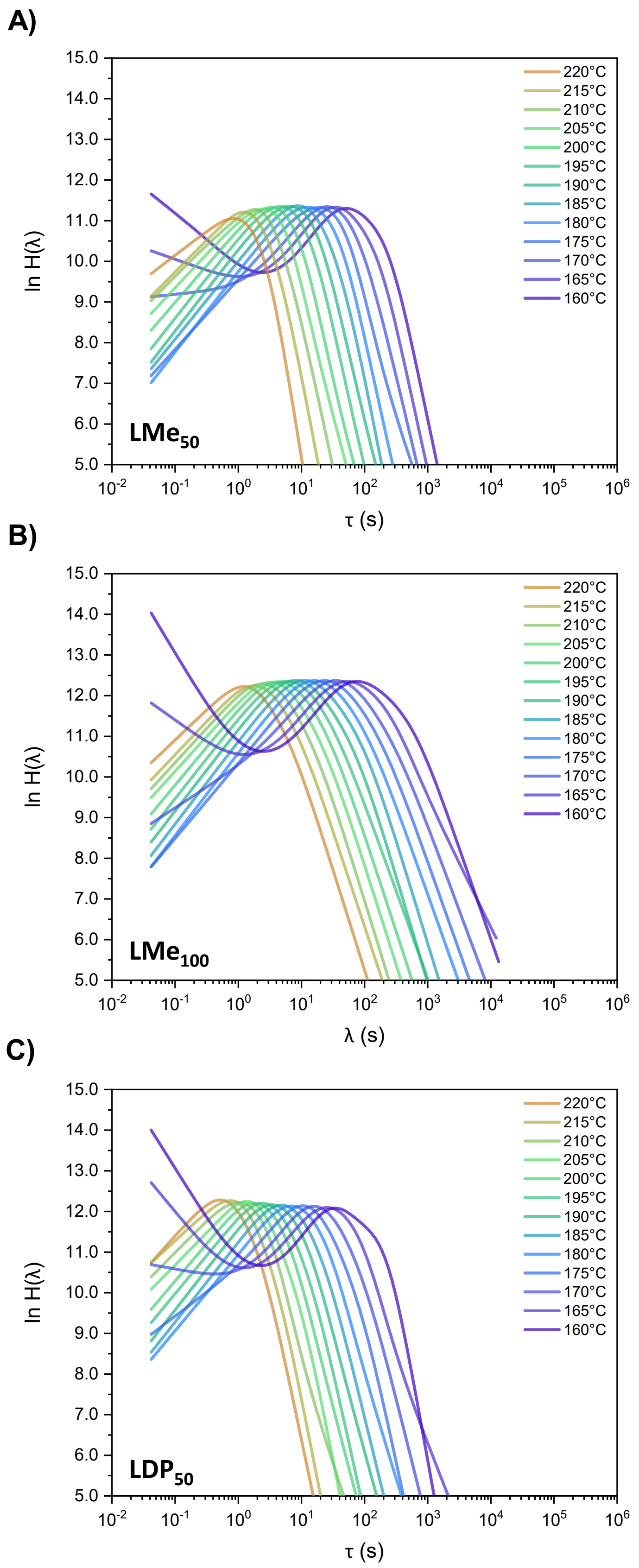

Figure S11. *H(λ)* distributions calculated from stress relaxation curves performed at temperatures ranging from 220°C to 160°C of networks: **A) LMe_{50}**, **B) LMe_{100}**, and **C) LDP_{50}**.

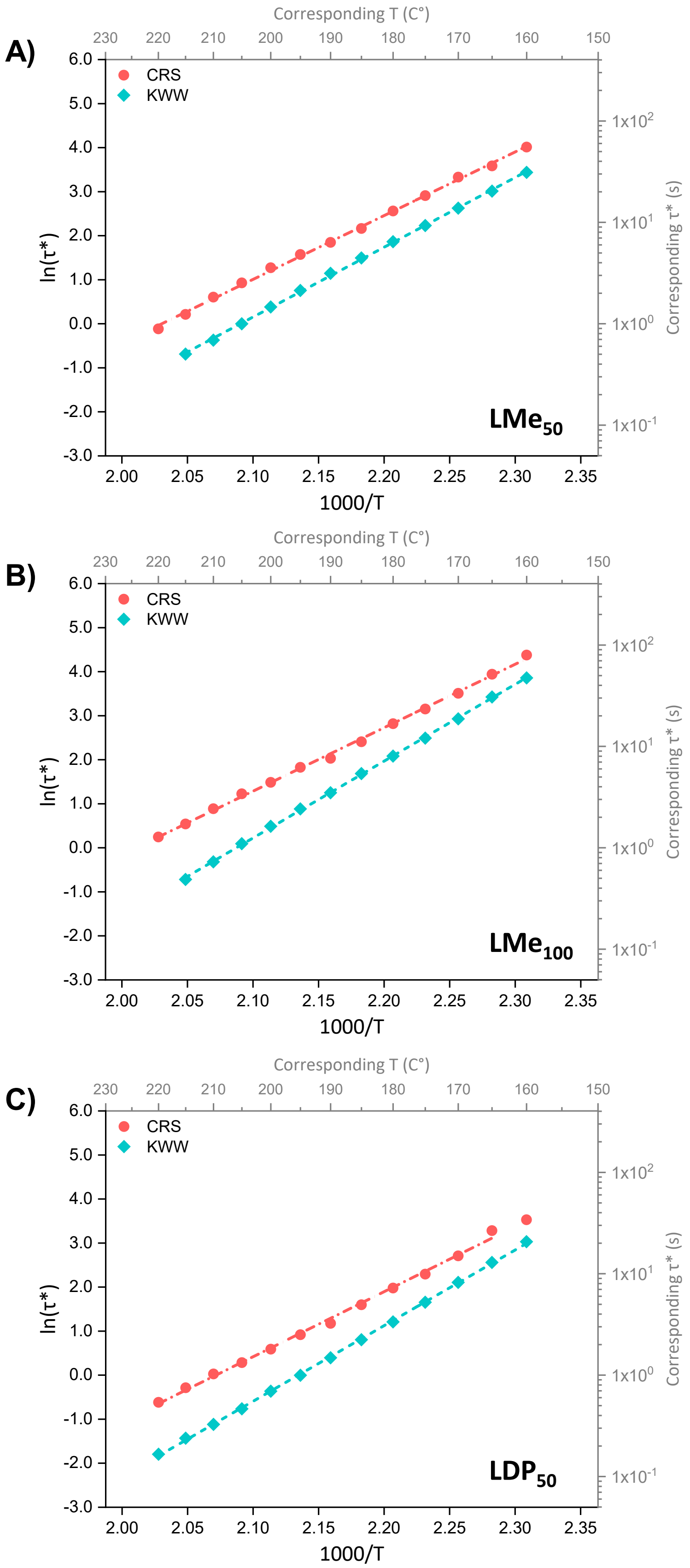

Figure S12. Stress relaxation Arrhenius plots of **PSMA$_L$** derived PS-MMA networks including CRS and KWW relaxation time-based plots ranging from 220°C to 160°C of networks.

The following fittings (**Figures S13-S18**) were made using a double Kohlrausch−Williams−Watts (KWW_D) stretched exponential decay ($Eq. S4$)[7] and continuous relaxation spectra (CRS) ($Eq. S2$).

$$G(t,T) = G_1 . e^{-\left(\frac{t}{\tau_1}\right)^{\beta_1}} + G_2 . e^{-\left(\frac{t}{\tau_2}\right)^{\beta_2}} \quad (Eq. S4)$$

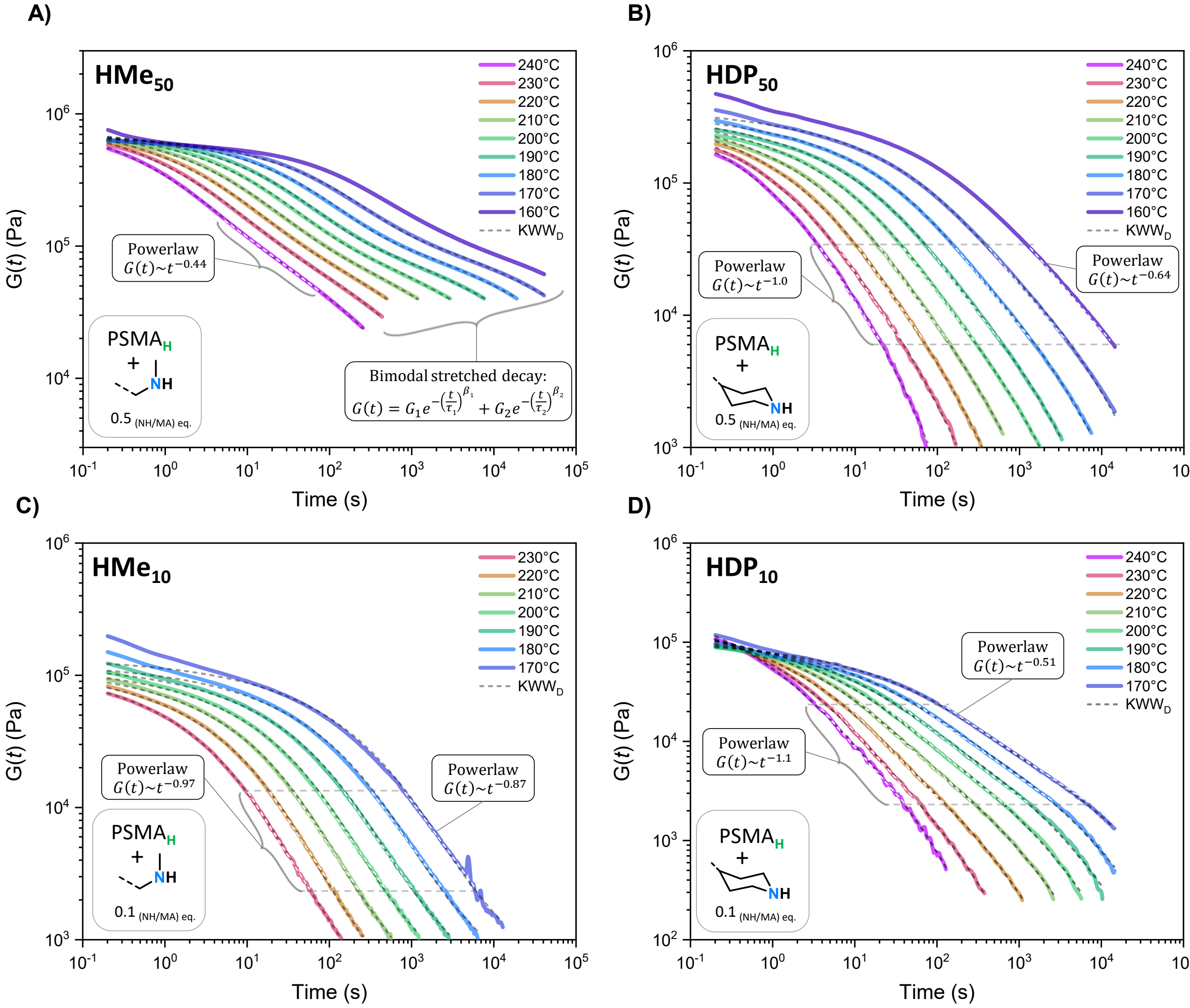

Figure S13. Stress relaxation curves performed at temperatures ranging from 210°C to 160°C of networks: **A) HMe$_{50}$, B) HDP$_{50}$, C) HMe$_{10}$** and **D) HDP$_{10}$,** with the corresponding overlayed KWW_D fits (gray dash lines).

Table S7. Stress relaxation β_1 values calculated by fitting the curves of **H**-Series materials to a two-element Kohlrausch–Williams–Watts (KWW$_D$) stretched exponential decay ($Eq. S4$).

Material	**β_1 at Temperature (°C)**							
	170	**180**	**190**	**200**	**210**	**220**	**230**	**240**
HMe$_{10}$	0.41	0.42	0.43	0.43	0.44	0.45	0.46	-
HMe$_{50}$	0.50	0.49	0.48	0.46	0.43	0.43	0.41	0.43
HDP$_{10}$	0.42	0.45	0.44	0.41	0.40	0.39	0.40	0.42
HDP$_{50}$	0.48	0.46	0.43	0.42	0.42	0.43	0.44	0.43

Table S8. Stress relaxation β_2 values calculated by fitting the curves of **H**-Series materials to a two-element Kohlrausch–Williams–Watts (KWW$_D$) stretched exponential decay ($Eq. S4$).

Material	**β_2 at Temperature (°C)**							
	170	**180**	**190**	**200**	**210**	**220**	**230**	**240**
HMe$_{10}$	0.20	0.19	0.21	0.21	0.22	0.24	0.25	-
HMe$_{50}$	0.19	0.18	0.17	0.17	0.17	0.17	0.18	0.18
HDP$_{10}$	0.20	0.21	0.21	0.21	0.21	0.22	0.23	0.25
HDP$_{50}$	0.20	0.24	0.24	0.24	0.24	0.24	0.25	0.26

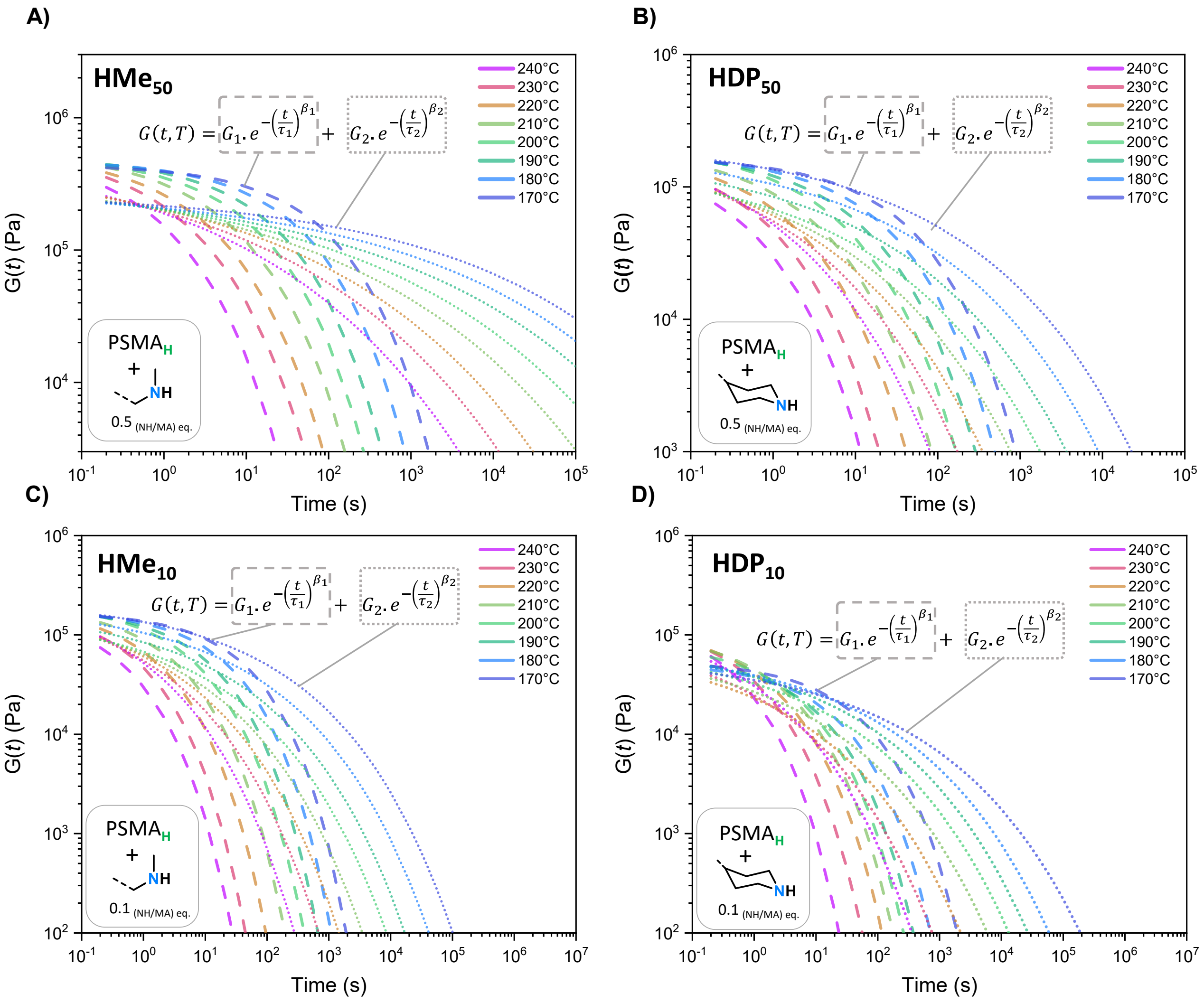

Figure S14. Separated bond-driven (dash lines) and Rouse-driven (dot lines) relaxation modes extracted from KWW_D fittings of stress relaxation curves performed at temperatures ranging from 210°C to 160°C of networks: **A) HMe$_{10}$, B) HMe$_{50}$, C) HDP$_{10}$** and **D) HDP$_{50}$**.

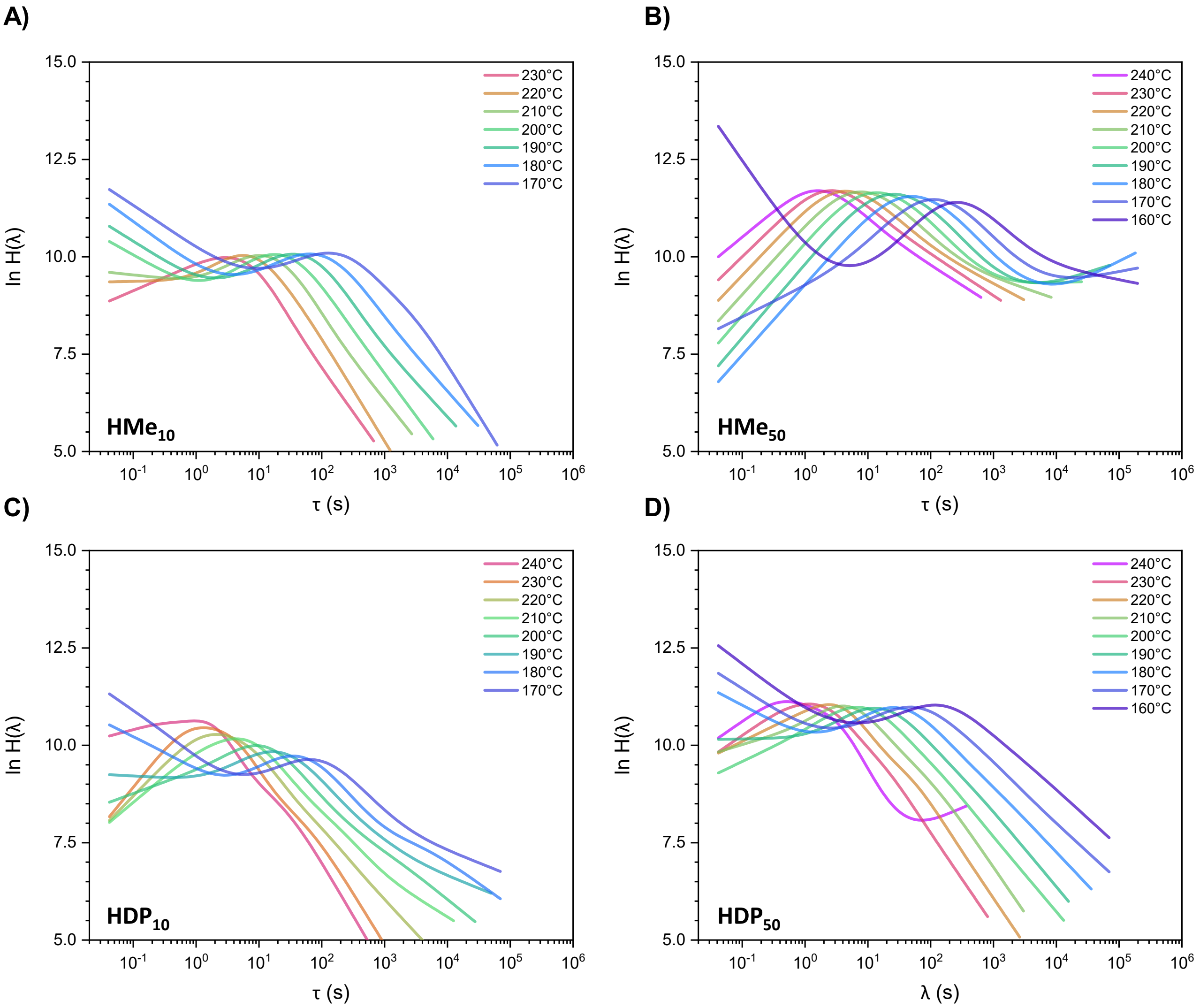

Figure S15. *H(λ)* distributions calculated from stress relaxation curves performed at temperatures ranging from 220°C to 160°C of networks: **A) HMe$_{10}$, B) HMe$_{50}$, C) HDP$_{10}$** and **D) HDP$_{50}$**.

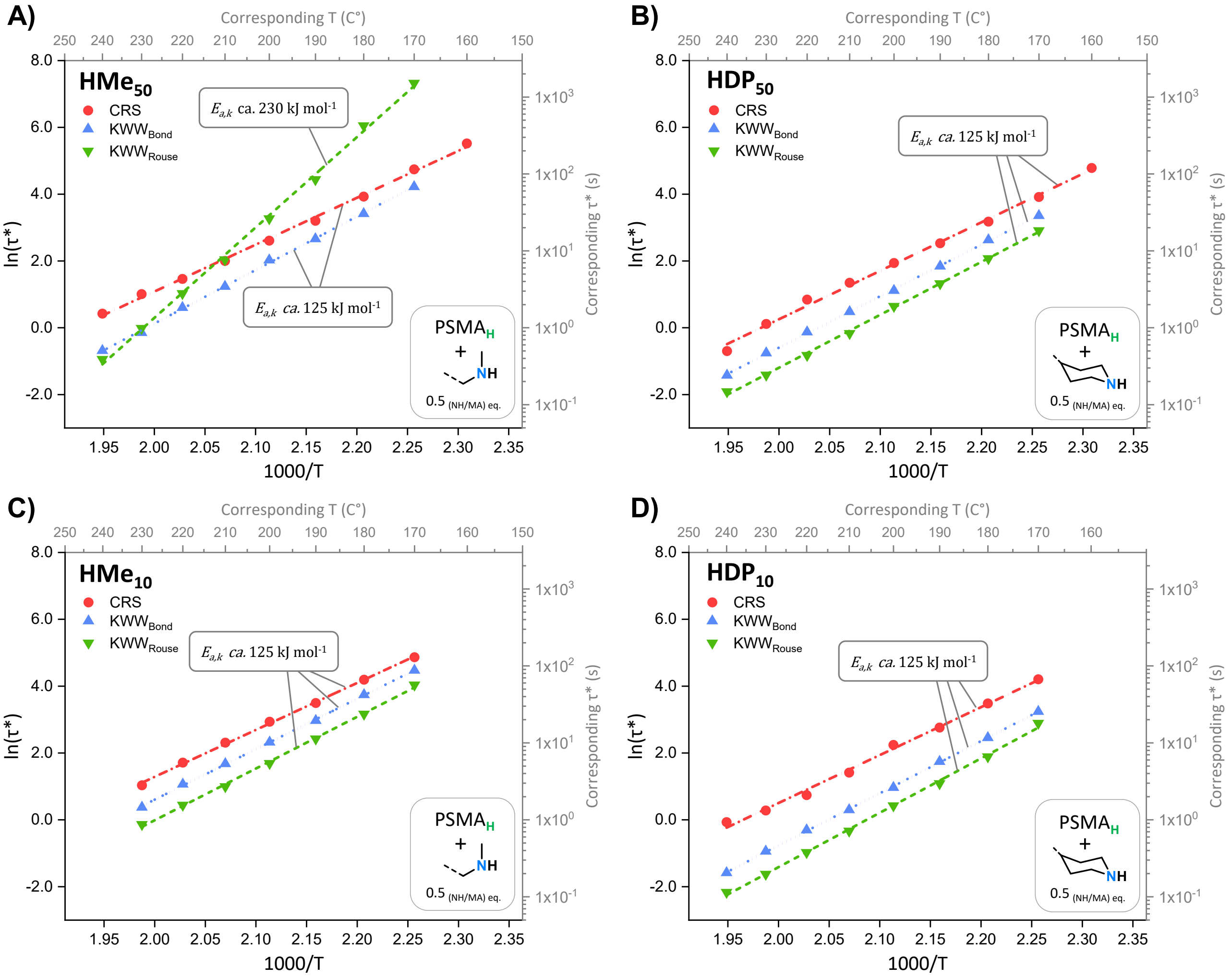

Figure S16. CRS (red circles), KWW$_{Rouse}$ (green inverted triangles) KWW$_{bond}$ (blue triangles) stress relaxation Arrhenius plots of PSMA$_H$ networks at temperatures ranging from 240°C to 160°C of networks: **A) HMe$_{10}$, B) HMe$_{50}$, C) HDP$_{10}$** and **D) HDP$_{50}$.**

Table S9. Stress relaxation results of **H**-Series materials calculated from the CRS $H(\lambda)$ maxima relaxation times and fitting their curves to a two-element Kohlrausch–Williams–Watts (KWW$_D$) stretched exponential decay equation ($Eq. S4$) and their R^2 values.

Network	$E_{a,k}$ (kJ mol^{-1})	R^2	$E_{a,k}$ (kJ mol^{-1})	R^2	$E_{a,k}$ (kJ mol^{-1})	R^2
	CRS		**KWW$_D$ Bond**		**KWW$_D$ Rouse**	
HMe$_{10}$	117 ± 1.8	0.999	126 ± 1.2	0.999	129 ± 1.4	0.998
HMe$_{50}$	117 ± 2.1	0.997	133 ± 2.6	0.999	229 ± 5.5	0.997
HDP$_{10}$	119 ± 3.3	0.995	130 ± 0.8	1.000	135 ± 2.3	0.998
HDP$_{50}$	121 ± 2.9	0.996	130 ± 1.7	1.000	132 ± 1.8	0.999

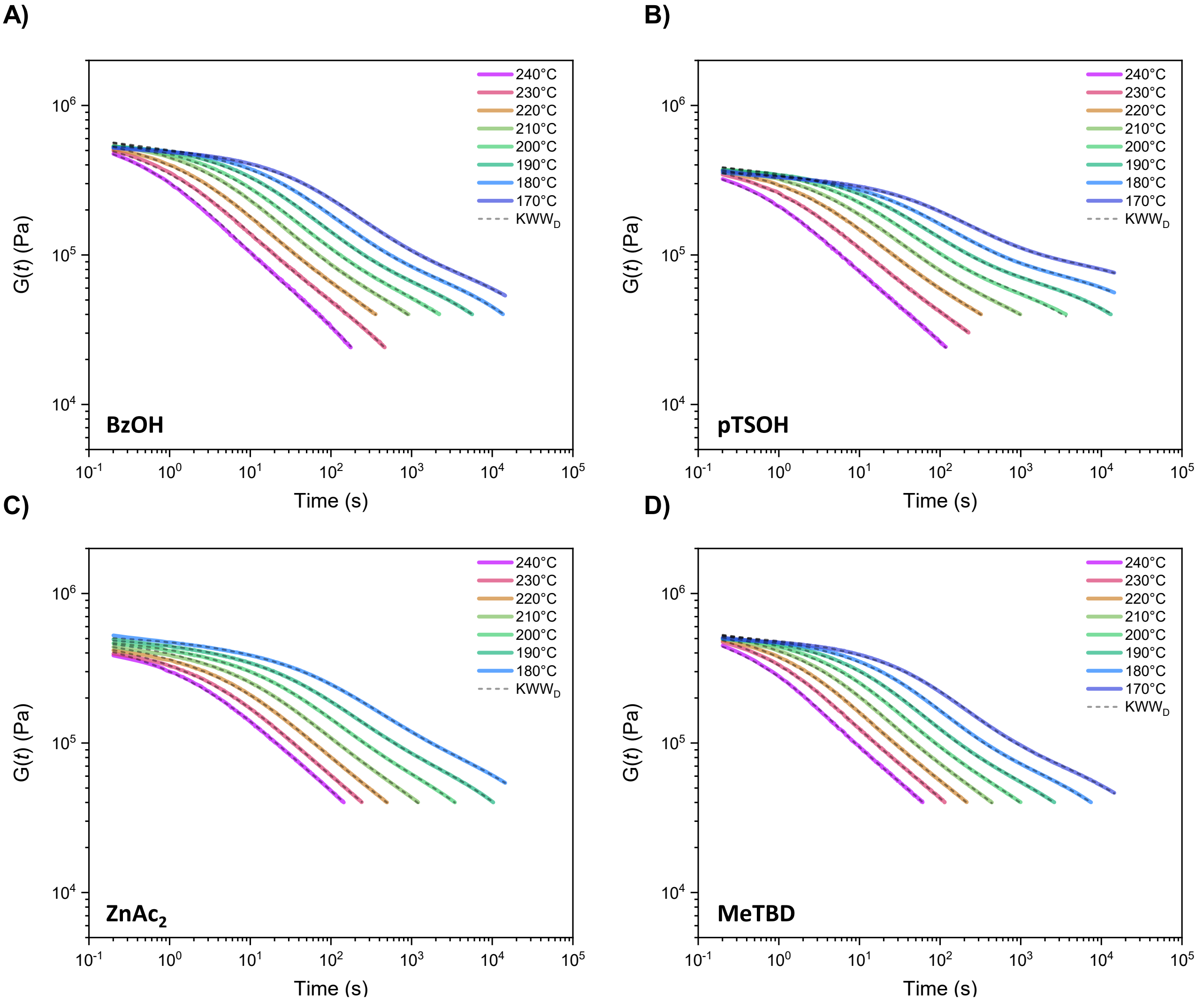

Figure S17. Stress relaxation curves performed at temperatures ranging from 210°C to 160°C of network **HMe$_{50}$** samples doped with: **A) BzOH**, **B) pTSOH**, **C) ZnAc$_2$** and **D) MeTBD**.

Table S10. Viscoelastic and rheological results of the original **HMe$_{50}$** (with no additional stickers) and **HMe$_{50}$** samples doped with rotation stickers obtained *via* SAOS and stress relaxation measurements.

Sticker	$G'_{p(220°C)}$[a] (kPa)	$G_{0(220°C)}$[b] (kPa)	$\tau_{220°C}$[c] (s)			$\tau_{180°C}$[d] (s)		
			CRS	**Bond**	**Rouse**	**CRS**	**Bond**	**Rouse**
None	440	596	4	2	3	51	30	424
BzOH	362	507	3	2	3	42	29	425
pTSOH	197	360	5	3	12	67	46	996
ZnAc$_2$	206	415	10	7	66	120	73	15497
MeTBD	391	484	3	2	1	36	29	223

[a] Apparent G' plateau values at 220°C. [b] $G(t,T)$ values at 220°C assuming: $G_0 = lim_{(t\rightarrow 0+)} G(t,T)$. [c,d] Relaxation times τ at 220 or 180°C obtained from CRS *H(λ)* maxima and both bond-driven and Rouse-driven KWW$_D$ components.

Table S11. Stress relaxation β_1 values calculated by fitting the curves of **HMe$_{50}$** samples doped with external reptation stickers to a two-element Kohlrausch–Williams–Watts (KWW$_D$) stretched exponential decay ($Eq. S4$).

Material	**β_1 at Temperature (°C)**							
	170	**180**	**190**	**200**	**210**	**220**	**230**	**240**
BzOH	0.49	0.48	0.46	0.44	0.44	0.43	0.43	0.44
pTSOH	0.50	0.49	0.47	0.49	0.44	0.44	0.42	0.44
ZnAc$_2$	-	0.44	0.46	0.46	0.46	0.43	0.42	0.41
MeTBD	0.52	0.52	0.50	0.50	0.50	0.50	0.50	0.51

Table S12. Stress relaxation β_2 values calculated by fitting the curves of **HMe$_{50}$** samples doped with external reptation stickers to a two-element Kohlrausch–Williams–Watts (KWW$_D$) stretched exponential decay ($Eq. S4$).

Material	**β_2 at Temperature (°C)**							
	170	**180**	**190**	**200**	**210**	**220**	**230**	**240**
BzOH	0.21	0.20	0.19	0.19	0.20	0.21	0.21	0.22
pTSOH	0.18	0.21	0.21	0.22	0.21	0.24	0.25	0.27
ZnAc$_2$	-	0.24	0.24	0.23	0.24	0.23	0.22	0.22
MeTBD	0.19	0.18	0.18	0.18	0.19	0.18	0.18	0.18

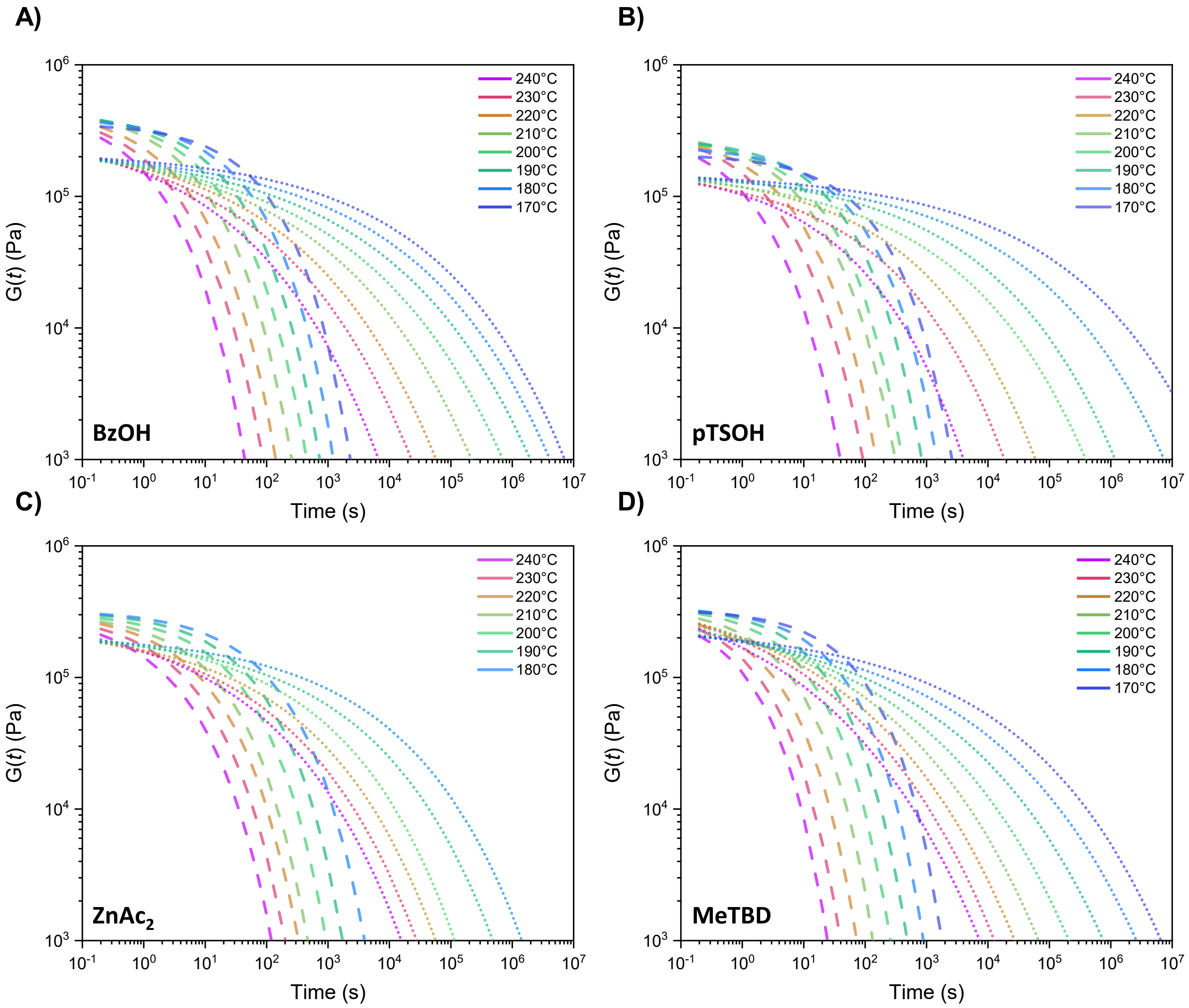

Figure S18. Separated bond-driven (dash lines) and Rouse-driven (dot lines) relaxation modes extracted from KWW$_D$ fittings of stress relaxatiFigureon curves performed at temperatures ranging from 210°C to 160°C of network **HMe$_{50}$** samples doped with: **A) BzOH**, **B) pTSOH**, **C) ZnAc$_2$** and **D) MeTBD**.

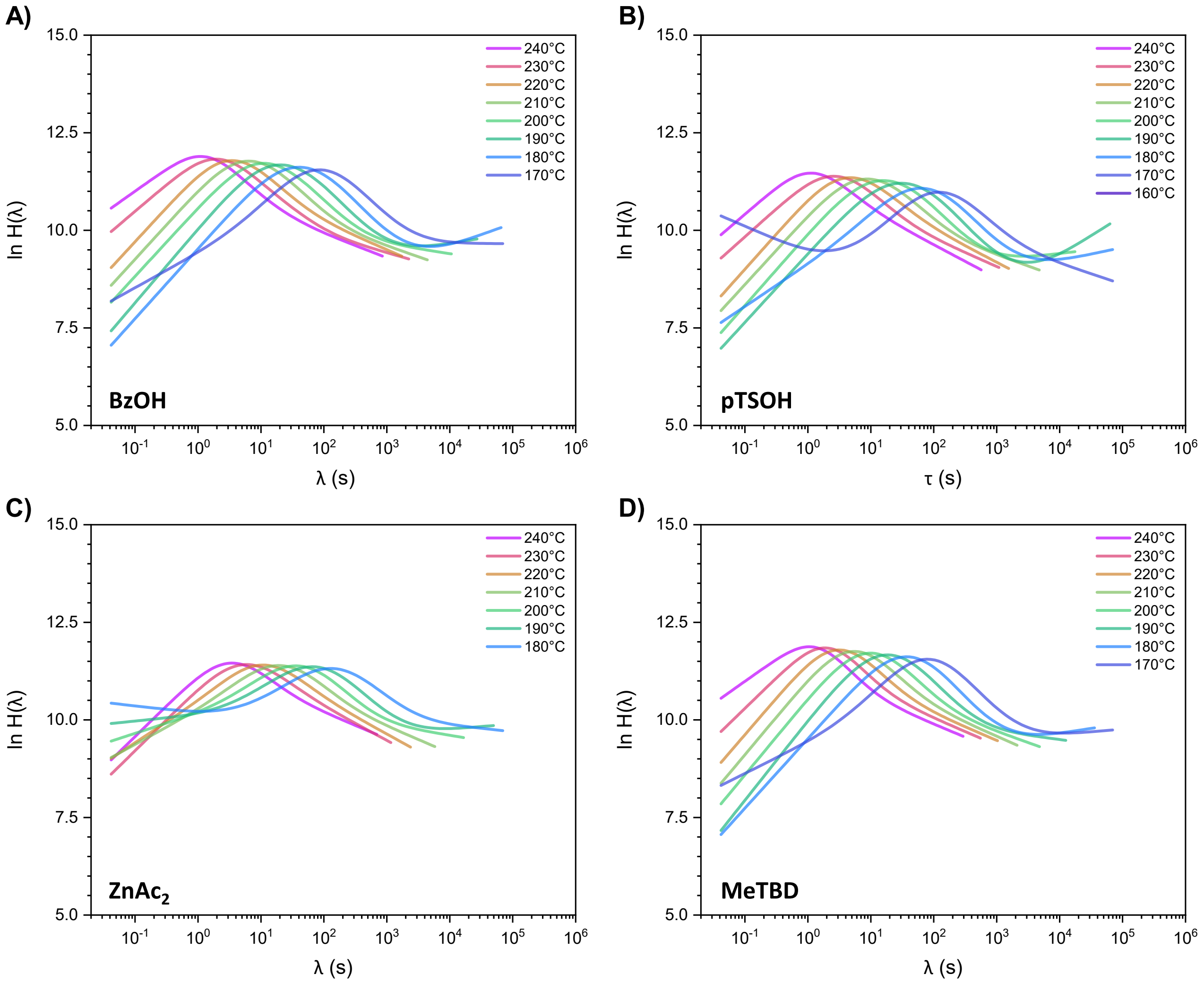

Figure S19. *H(λ)* distributions calculated from stress relaxation curves performed at temperatures ranging from 220°C to 160°C of network **HMe_{50}** samples doped with: **A) BzOH**, **B) pTSOH**, **C) $ZnAc_2$** and **D) MeTBD**.

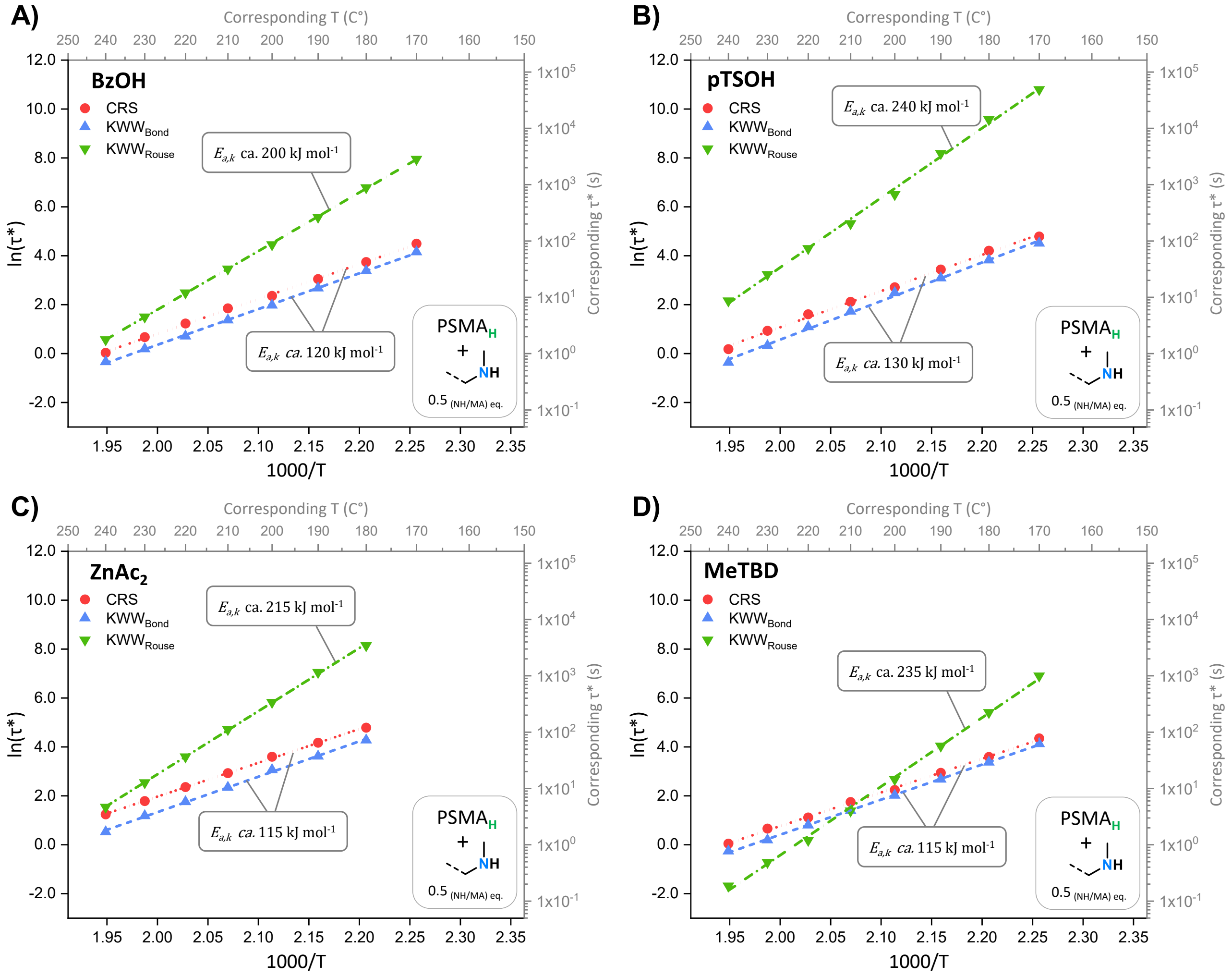

Figure S20. CRS (red circles), KWW$_{Rouse}$ (green inverted triangles) KWW$_{bond}$ (blue triangles) stress relaxation Arrhenius plots of PSMA$_H$ networks at temperatures ranging from 240°C to 160°C of network **HMe$_{50}$** samples doped with: **A) BzOH**, **B) pTSOH**, **C) ZnAc$_2$** and **D) MeTBD**.

Table S13. Stress relaxation values of **HMe$_{50}$** samples doped with external stickers calculated from the CRS $H(\lambda)$ maxima relaxation times and fitting their curves to a two-element Kohlrausch–Williams–Watts (KWW$_D$) stretched exponential decay equation ($Eq. S4$) and their R^2 values.

Sticker	$E_{a,k}$ (kJ mol^{-1})	R^2	$E_{a,k}$ (kJ mol^{-1})	R^2	$E_{a,k}$ (kJ mol^{-1})	R^2
	CRS		**KWW$_D$ Bond**		**KWW$_D$ Rouse**	
None	117 ± 2.1	0.997	133 ± 2.6	0.999	229 ± 5.5	0.997
BzOH	118 ± 1.4	0.999	126 ± 1.2	0.999	129 ± 1.4	1.000
pTSOH	131 ± 2.7	0.997	133 ± 2.6	0.997	229 ± 5.5	0.997
ZnAc$_2$	115 ± 1.2	0.998	130 ± 0.8	0.999	135 ± 2.3	1.000
MeTBD	114 ± 1.6	0.999	130 ± 1.7	0.999	132 ± 1.8	0.998

5.3. Creep measurements

The macroscopic flow behavior of PS-MME-based CANs was evaluated *via* creep analysis. In this process, a steady viscous flow is generated and monitored on a material under a defined and constant shear stress. Once the elastic buildup reaches its full extent, assuming the sample follows the Burgers model for viscoelastic deformations,[8] the observed steady flow is then comparable to that of a viscous liquid and can be used to calculate its zero shear viscosity (η_0) (**Figure S21**).[3,9] Then from there, the $E_{a,v}$ can be calculated following equation ($Eq. S5$).

$$\eta_0(T) = \left(\frac{dJ(T,t)}{dt}\right)^{-1} = A_\eta . e^{\frac{E_{a,v}}{RT}} \ (Eq. S5)$$

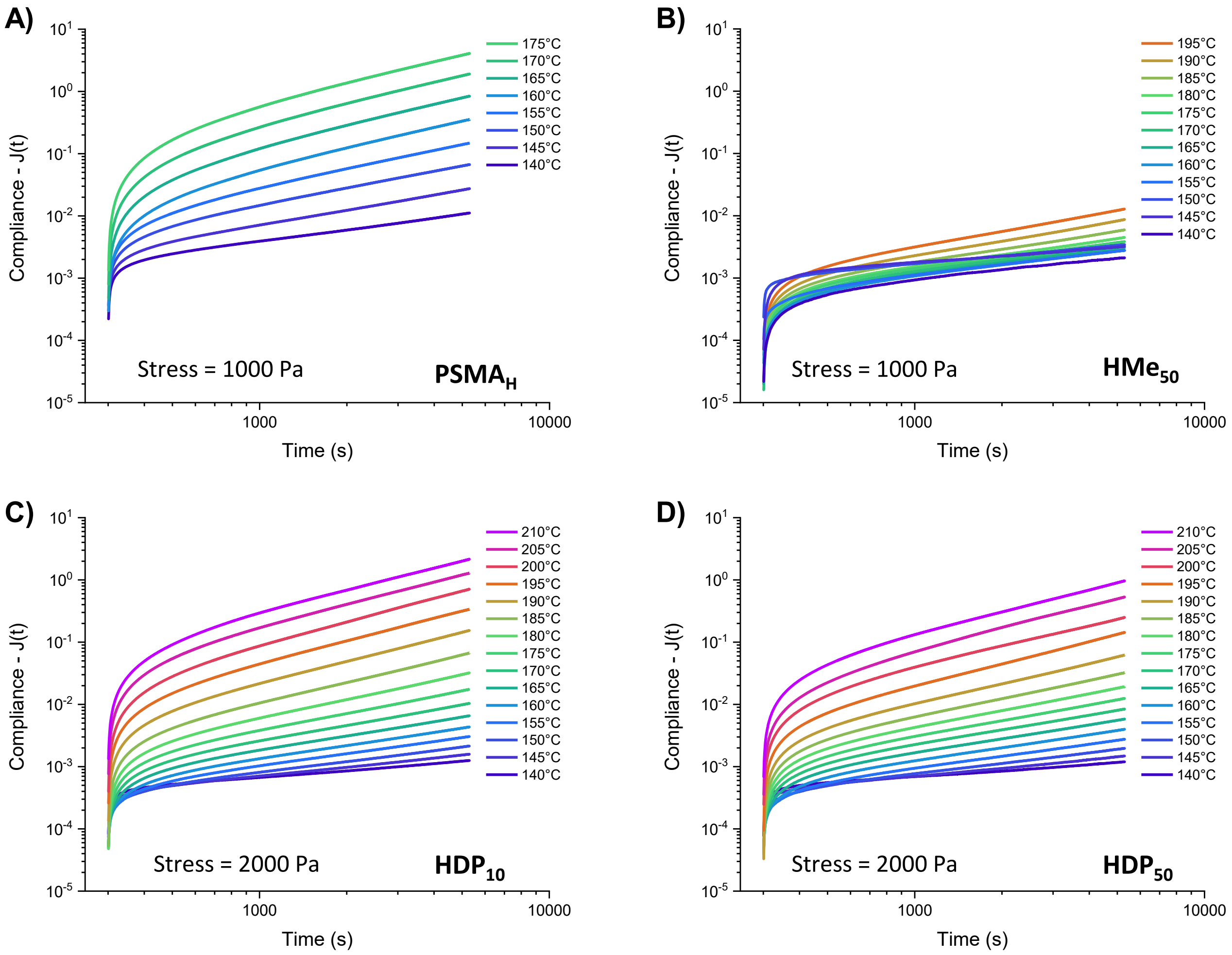

Figure S21. Creep compliance curves of experiments performed at temperatures ranging from 140°C to 210°C of PS-MMA networks: **A) PSMA$_H$, B) HMe$_{50}$, C) HDP$_{10}$** and **D) HDP$_{50}$.**

Table S14. Viscous flow activation energies on creep $Regimes\ I$ and II and their R^2 values.

Material	$E_{a,v}^{I}$ [a] (kJ mol^{-1})	R_I^2 [b]	$E_{a,v}^{II}$ [c] (kJ mol^{-1})	R_{II}^2 [d]
PSMA$_H$	-	-	275 ± 2.3*	0.999
HMe$_{50}$	22 ± 5.1	0.865	155 ± 4.0	0.998
HDP$_{10}$	139 ± 1.4	0.987	261 ± 6.9	0.999
HDP$_{50}$	138 ± 2.8	1.000	265 ± 5.9	0.997

[a,c] Viscous flow activation energies ($E_{a,v}$) of networks on flow $Regimes\ I$ or II calculated from equation ($Eq. 6$). [b,d] Coefficient of determination (R^2) of $E_{a,v}$ in flow *Regimes I* or *II*. * This $E_{a,v}$ does not correspond to a material on *Regime II* as it does not exhibit dynamic crosslinks. It has been included to serve as a comparison between the PS-MMEs on such flow regime and their polymer precursor.

6. Injection molding experiments

Figure S22. Pictures of **A)** Rectangular geometry mold (63.5 mm x 12.5 mm x 3.15 mm) used during injection molding experiments. **B)** DSM Mini Injection Molding machine used for the extrusion experiments.

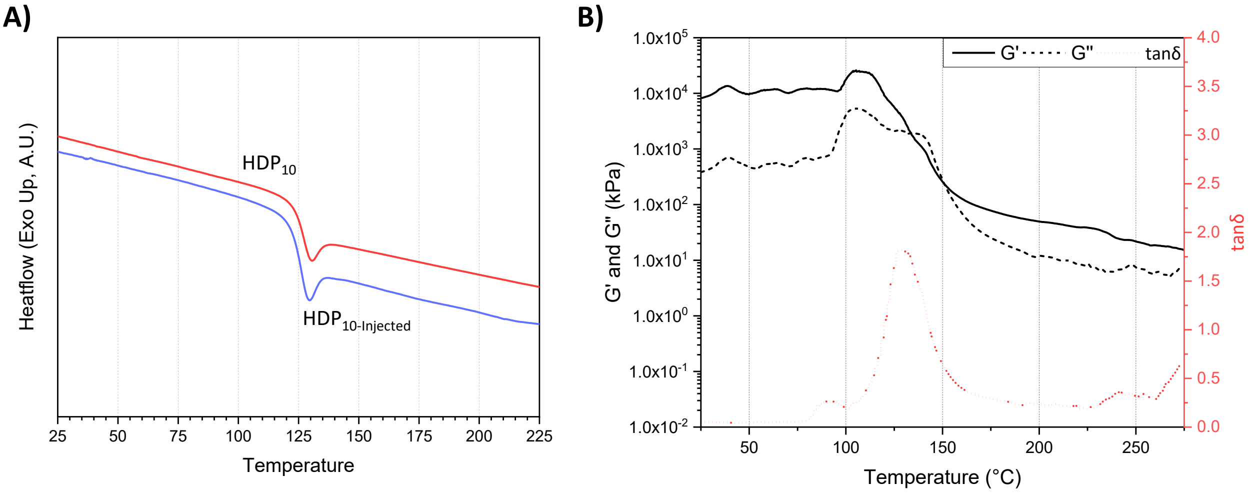

Figure S23. **A)** DSC thermograms of network **HDP$_{10}$** as synthesized (red) and after its injection molding at 280 °C (blue), showing no observable changes due to processing. **B)** DMTA thermogram of the injected **HDP$_{10}$** network specimen.

7. Network solubility and chemical recycling experiments

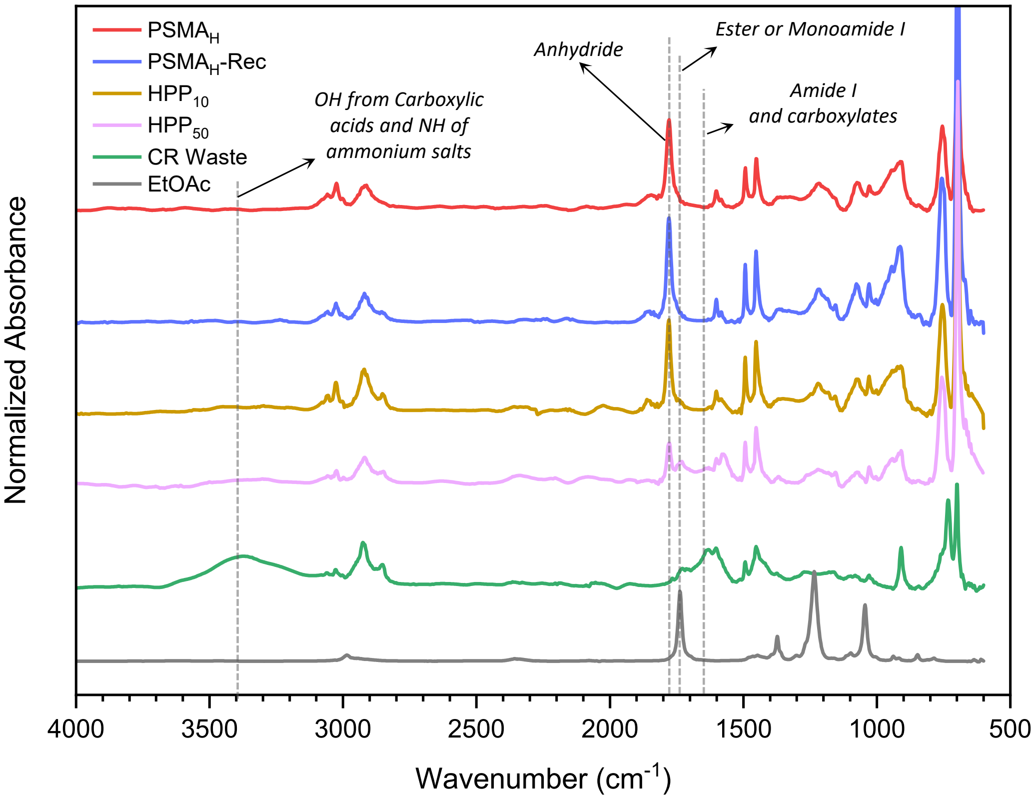

Figure S24. FT-IR spectra of virgin **PSMA$_H$** (red), **PSMA$_H$** recovered from the chemical recycling of **HDP$_{10}$** (cyan), **HDP$_{10}$** (ocher), **HDP$_{50}$** (pink), the chemical recycling waste (CR Waste) separated from the last precipitation (green) of the recycled **PSMA$_{H\text{-}Rec}$** and ethyl acetate (EtOAc) as an aliphatic ester reference (gray).

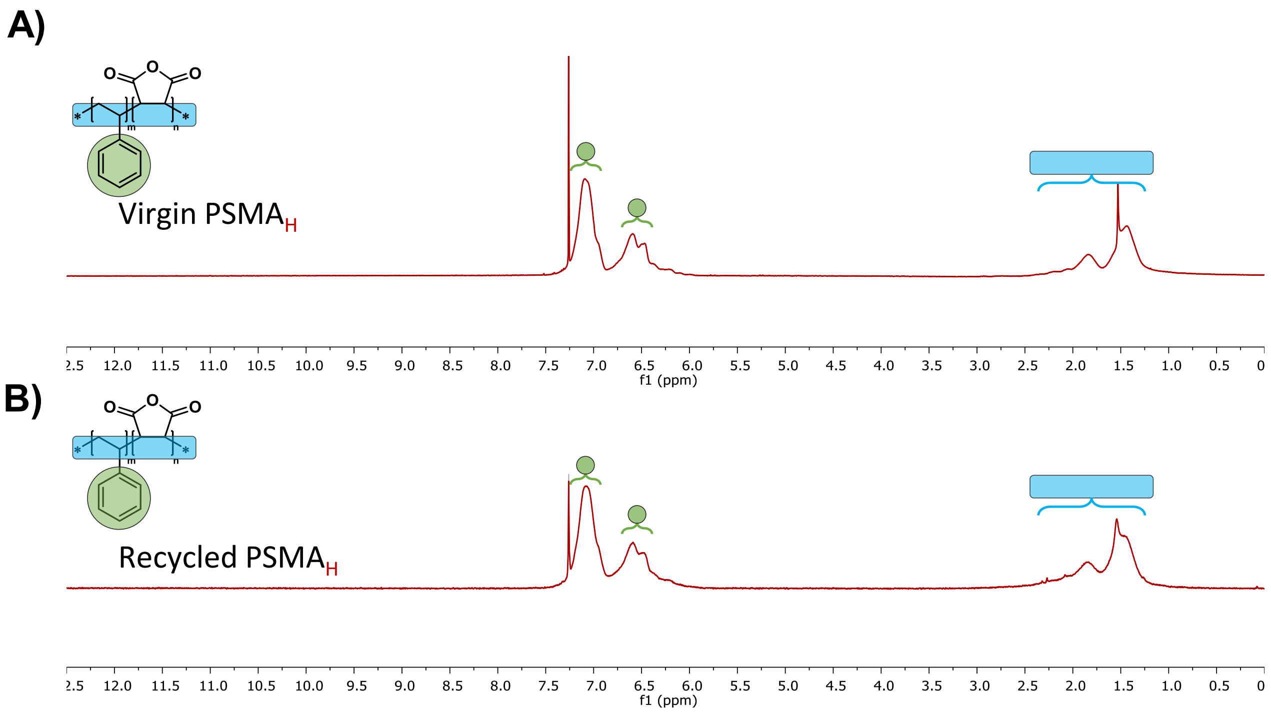

Figure S25. ^{1}H-NMR spectra of **A)** virgin **PSMA$_{H}$** and chemically recycled **PSMA$_{H\text{-}Rec}$**.

8. References

1 F. F. Becker, C. Mukhopadhyay, L. Hackfeld, I. Banik and B. K. Banik, *Bioorg. Med. Chem.*

2 V. Zhang, B. Kang, J. V. Accardo and J. A. Kalow, *J. Am. Chem. Soc.*, 2022, jacs.2c08104.

3 A. Jourdain, R. Asbai, O. Anaya, M. M. Chehimi, E. Drockenmuller and D. Montarnal, *Macromolecules*, 2020, **53**, 1884–1900.

4 L. E. Porath and C. M. Evans, *Macromolecules*, 2021, **54**, 4782–4791.

5 S. Shanbhag, *Macromolecular Theory and Simulations*, 2019, **28**, 1900005.

6 M. Mours and H. H. Winter, in *Experimental Methods in Polymer Science*, ed. T. Tanaka, Academic Press, Boston, 2000, pp. 495–546.

7 R. G. Ricarte and S. Shanbhag, *Polym. Chem.*, 2024, **15**, 815–846.

8 A. M. Hubbard, Y. Ren, C. R. Picu, A. Sarvestani, D. Konkolewicz, A. K. Roy, V. Varshney and D. Nepal, *ACS Appl. Polym. Mater.*, 2022, **4**, 4254–4263.

9 F. Van Lijsebetten, T. Debsharma, J. M. Winne and F. E. Du Prez, *Angewandte Chemie International Edition*, 2022, **61**, e202210405.